OPTICAL INVESTIGATION OF LASER PEENING

By

Dilhan K. L. Don-Liyanage

An MPhil Thesis

Submitted in partial fulfilment of the requirements for the award of
Master of Philosophy at Loughborough University

December 2001

Acknowledgements

I would like to take this opportunity to thank all the people who have supported me and helped me in achieving this thesis. Without their help I wouldn't have reached this far.

Firstly, I would like to thank my supervisor Professor D. C. Emmony for giving me the opportunity to work for this degree. He was always available to help, support and guide me through any difficulties I faced and always found time to have interesting discussions with me relating to the thesis.

Many thanks also go to the students and staff in the Physics Department especially John Oakley for his help with the construction of mechanical parts and preparation of the samples.

I would also like to thank all my friends in Loughborough and all around the world who encouraged me.

Last, but not least, I want to thank my parents who had made possible for me to be where I am. Dedicating this work to them is the least I can do.

Dedicated to my Parents

Abstract

Laser hardening or laser peening involves the interaction of an intense laser pulse with the absorbing surface of the metal under water. An ablation shockwave is produced which, depending on the geometry and laser beam area, induces residual stress on the surface layer of the metal. The aim of the research work presented in this thesis is to investigate optically the laser peening method by analyzing the ablation shock waves using high-resolution Schlieren photography.

The laser used to peen the surface of the metal was a near infra red Q-switched Nd:YAG laser with a energy output per pulse of 600mJ, pulse duration of 13 ns and a wavelength of 1064nm. The metal surface to be peened was placed just below the water surface in a tank filled with distilled water. The Nd:YAG laser beam was focused on the surface of the metal which was painted black to make it strongly absorbing to the laser radiation. The ablation shock wave produced is reflected and transmitted through the metal. This event is photographed using a digital camera with a 1.8Mpixel CCD (Minolta RD175), combined with a Schlieren technique to enable visual observation of the acoustic shockwaves in the water. The light source was a nitrogen-pumped dye-laser with pulse duration of ~0.5ns, which ensured no blurring of the final image.

Laser peening was optically investigated with aluminium, copper, steel, brass, titanium and stainless steel shims. Different thicknesses of paint were applied to the surface of copper and stainless steel in order to observe the effect on the shock waves produced. Using an appropriate thickness of stainless steel shim it was possible to produce ultrasound in water using the Laser shock peening process. In some experiments a series of high frequency waves were seen in the water.

Content

CHAPTER 3: Laser Induced Cavitation

CHAPTER 4: The Laser Peening Process

CHAPTER 5: Shims

CHAPTER 6: Ultrasonic Fringes

CHAPTER 1

Introduction

1-1 The Laser

In 1960, electronic scientists and engineers began to see things in a different light. It was a rich ruby light, emitted by the atom of a synthetic gemstone. The light came from the laser, a new device with wide potential application in science, medicine, industry and national defence. The word LASER is an acronym and stands for Light Amplification by Stimulated Emission of Radiation. It was joined by analogy to MASER "Microwave Amplification by Stimulated Emission of Radiation" (Bertolotti, 1983).

The laser was one invention, which was not stumbled upon accidentally but was developed by design and can perhaps trace its descent from Einstein, who advanced the concept of stimulated emission of radiation in 1917 (Einstein, 1917). He pointed out that the equation proposed by Planck to describe the spectral distribution of light emitted from a black body could be derived quite simply by assuming the existence of a light emitting process which has since become known as stimulated emission (Bertolotti, 1983).

The ancestor of the laser was the maser. The maser amplified electromagnetic radiation of much longer wavelength in the microwave range. The motivation for the development of the maser seems to be the interest in microwave radiation following the utility it found in World War II. The first Maser was created by Charles H. Townes (1954) who along with James Gordon and Herbert Zeiger succeeded in producing an inverted population by isolating excited ammonia molecules. The excited molecules were aimed into a cavity resonant at the 24-Gigahertz frequency of the ammonia transition where stimulated emission occurred.

Soon after the maser became reality, people began to look at the possibility of stimulated emission in other regions of the electromagnetic spectrum. Townes, along with Arthur Schawlow, began investigating the possibility of optical and IR masers. The invention of the laser can be dated to December 1958 with the publication of the scientific paper, Infrared and Optical Maser, by Arthur L. Schawlow (1958), then a Bell Lab researcher, and Charles H. Townes, a consultant to Bell Labs. It was not until 1960 that Theodore Maiman (1960) created the first working laser. Maiman's laser was a "pink" ruby rod with its ends silvered, placed inside a spring-shaped flash lamp. Maiman's laser was only capable of pulsed operation due to its 3 energy level transition. In 1960, Peter Sorokin and Mirek Stevenson (Bertolotti, 1983) developed the first 4-level laser, which was capable, in theory, of continuous output action. Just before the end of 1960 (published 1961), Ali Javan, William Bennet, and Donald Herriot (Bertolotti, 1983) made the first gas laser using helium and neon. This type of laser (a He-Ne laser) became the dominant laser for the next 20 years until cheap semiconductor lasers took over in the mid-80's. The He-Ne laser was the first laser to emit a continuous beam and the lasing action could be initiated by an electric discharge rather than the intense discharge of photons from a flash lamp.

The light emitted by a laser is remarkable for being coherent: it is composed of regular and continuous waves, like those emitted at much lower frequencies by radio transmitters, and in this respect it differs from the incoherent light emitted by other sources of light such as stars, candle or electric lamps

First built in 1960, lasers now range in size from semiconductor lasers as small as a grain of salt to solid-state and gas lasers as large as a warehouse. The light beam produce by most lasers is pencil-thin and maintains its size and direction over very large distances. Lasers are widely used in industry for cutting and boring metals and other materials, in medicine for surgery, and in communication, scientific research, and holography. The potential for lasers developed faster in the field of medicine after Kumar Patel (Bertolotti, 1983) of Bell Labs in 1964 invented the carbon dioxide laser, which soon permitted surgeons to perform highly intricate surgery using photons, rather than scalpels, to both operate on and cauterize wounds. Lasers today can be inserted inside the body, performing operations that a few years ago were almost impossible to perform, at little risk or discomfort to the patient.

Whether lasers provide the energy that ignites a fusion reaction in isotopes of hydrogen, scan bar codes on produce in a supermarket, or provide the light source for high-capacity telecommunications systems, they all operate according to the basic principles put forth by Schawlow and Townes at Bell Labs in 1960's. The laser has contributed to humanity as a powerful scientific tool for expanding human knowledge and in its many applications that helped people directly.

"A splendid light has dawned on me..." - Albert Einstein

Type	Wavelength (μm)	Efficiency	Power levels available (W)	
			Pulsed	CW
CO_2	10.6	0.01-0.02 (pulsed)	$> 2 \times 10^{13}$	$> 10^5$
CO	5	0.4	$> 10^9$	> 100
Holmium	2.06	0.03(lamp) 0.1 (diode)	$> 10^7$	30
Iodine	1.315	0.003	$> 10^{12}$	-
Nd-glass, YAG	1.06	0.001-0.06(lamp) > 0.1 (diode)	$\sim 10^{14}$ (10 beams)	$1 - 10^3$
* Colour centre	1 - 4	10^{-3}	$> 10^6$	1
*Vibronic (Ti Sapphire)	0.7 - 0.9	$> 0.1 \times \eta_p$	10^6	1 - 5
Ruby	0.6943	$< 10^{-3}$	10^{10}	1
He-Ne	0.6328	10^{-4}	-	$1 - 50 \times 10^{-3}$
* Argon ion	0.45 - 0.60	10^{-3}	5×10^4	1 - 20
* OPO	0.4 - 9.0	$> 0.1 \times \eta_p$	10^6	1 - 5
N_2	0.3371	0.001 - 0.05	$10^5 - 10^6$	-
* Dye	0.3 - 1.1	10^{-3}	$> 10^6$	140
Kr - F	0.26	0.08	$> 10^9$	500
Xenon	0.175	0.02	$> 10^8$	-

Table 1.1 Efficiencies and power levels of lasers*= Tuneable sources, η_p=pump laser efficiency. YAG stands for Yttrium Aluminium Garnet and OPO for Optical Parametric Oscillator.

1-2 High Speed Photography

The beginning of high speed photography might be considered to be William Henry Fox Talbot's (1852) experiment in 1851. He attached a page of the London Times newspaper to a wheel, which was rotated in front of his wet plate camera in a darkened room. As the wheel rotated, Talbot exposed a few square inches of the newspaper page for about 1/2000th of a second, using spark illumination from Leyden jars. This experiment resulted in a readable image.

The human eye in combination with the brain is limited when observing rapidly changing phenomena. If the phenomena is recorded by frames at rates faster than 10 to 12 times per second the eye is not able to resolve the fast moving phenomena and therefore recognises it as a continues process. However, due to these limitations of the eye, the observation of very fast moving objects such as a shock wave propagating in a liquid, needs special equipment which allows the extension of the time scale of an event. This is the role of high speed photography which firstly allows us to observe things not normally perceived by the naked eye and secondly provides the power to manipulate time.

The development of high speed photography was dependent upon improvements in ordinary still photography. Although many ideas of high speed photography were suggested and while many were feasible they were not able to be realised until the technology of still photography had been developed.

Up to the turn of the century, spark photography was the primary method employed in high speed photography because of the short exposure time which could be achieved. After getting single photographs there were a desire to photograph a visual history of short duration events. For this, multiple sequential sparks and improved shutters with faster operating times were necessary. The first spark system associated with a drum camera driven by an engine was set up in France in 1904. It produced up to 2000 sparks per second with the camera giving up to 50 full size images. Photographs of insects in flight and flying bullets were taken with this technique (Anon, 1920).
The first high speed photography cameras were used in such areas as animal movement, flow visualisation and ballistic events. One of the industrial applications

of high speed photography was as a fault finding tool for electrical relays. One problem at this time was the lighting of the high speed events. Sparks were as short as 100 ns, but their luminosity was not high enough to illuminate the event. On the other hand bright high speed xenon lamps emitted a light pulse not shorter than 1μs. The use of other alternative methods, a Kerr cell shutter and an argon flash bomb, were discussed in the mid – 1930s but were not used until World War II (Beams, 1930).

Since the introduction of high speed photography in 1851 by Fox Talbot (1852) the technique has covered a wide range of areas. Lighting in high speed photography is of particular importance due to the high framing rates and the very short exposure times which can be as low as picoseconds in some cases to achieve high temporal resolution. Another very important application of light in high speed photography is the use of very short duration flash lights as an alternative to mechanical or electrical shutters in cameras. The cameras with an open shutter are positioned in a dark room and the images are exposed by illuminating the object for a short time as in the current experimental work.

The first experiments of high speed photography were carried out approximately 150 years ago. Since then camera technique has been developed enormously. As the events of interest have tended towards shorter and shorter durations mechanical cameras reached their limits and electro-mechanical or purely electronic cameras have evolved to cope with extremely short exposure times. It is possible to proceed from image capture to hard copy printout via electronic cameras and computers without using a wet film. But because of the resolution achieved with wet film, which is still far better than for electronic cameras (Gentry, 1997), it is expected that film and electronic recordings will proceed as complementary systems. The growth of electronic systems in the field of high speed photography needed to include the term "photonics" as well and the subject is now usually referred to as "high speed photography and photonics".

1-3 Shock Waves

Shock waves have fascinated scientists for many years. Before the discovery of explosives, the commonly encountered shock waves were in thunder. Until the 17^{th} century such violent phenomena were covered in mystery and they were related to evil powers. Now we know that shock waves are created by a very sudden release of chemical, electrical, nuclear or mechanical energy in a limited space. In nature, the most frequently encountered shock wave is the thunder that follows the lightning. Shock waves are also associated with earthquakes and volcanic eruptions. Typical man made shock waves result from the detonation of explosive materials, and also complex shock wave structures appear in supersonic flights. These all can range from weak shock waves associated with the use of any firearm up to shock waves resulting from nuclear explosions reaching enormous magnitudes. In descriptive terms, a shock wave is a very sharp, thin front in a fluid through which there exists a sudden change in all flow properties, such as pressure, temperature, density, velocity and entropy.

It has been known for some time that the linear treatment of sound waves or phenomena that can be represented by a linear differential equation no longer applies when the amplitude of the disturbance becomes large. In shock wave phenomena, shock fronts are seen which are extremely rapid changes in the thermodynamic state of the fluid medium. Shock fronts can occur at some later time in a flow, which was initially continuous, and are then able to propagate without further change. It is the propagation of shock fronts through the medium, which is usually referred to as the shock wave so that the usual association of the term 'wave' with periodic motion is lost.

The realisation that shock waves are physically possible can be attributed to Earnshaw in the year 1858 (Earnshaw, 1860). Two years later, a theory describing the propagation of such waves, which assumed an adiabatic, reversible transition, was derived independently by Riemann (1876) using an elegant treatment which has since become known as the method of Riemann invariants. Rankine (1870) examined this theory further and showed that the process could not be adiabatic as Riemann had assumed. However, the nature of the process still remained uncertain until Rayleigh and Hugoniot (Rayleigh, 1910 and Hugoniot, 1889) both demonstrated that such transitions must involve a change of entropy and therefore could be neither adiabatic nor reversible.

The theory of shock waves is a vast subject, involving many branches of physics and chemistry. Shock waves have received especially great attention because modern aerodynamics deals with objects moving at velocities which approach and exceed the sound velocity. In addition, shock waves, as previously mentioned, are produced in explosions. A clear idea of shock wave formation and propagation is essential to investigation of the explosion mechanism itself.

In the following experimental work, shock waves are observed in the oscillatory motion of a cavity. When a bubble is produced in water by focusing a high power laser beam, it produces plasma in the water, which in turn produces an expanding cavity and a first shock wave. A second shock wave is seen when the cavity reaches minimum radius and collapses before going into the expanding oscillatory behaviour (more detail in Chapter 3). Shock waves are also seen in the laser shock peening, where the shock wave is used in the peening process (Chapter 4). Interaction of a high power laser pulse with the paint layer on the surface of the metal produces a shock wave, which propagates inside the metal as well as in the surrounding water.

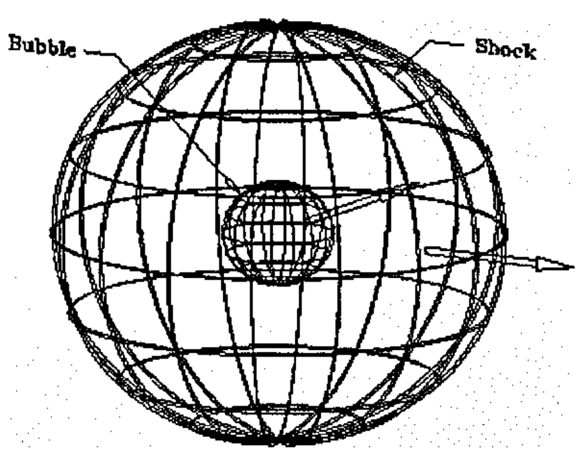

Figure 1.1 Schematic diagram of an expanding spherical shock wave generated by an expanding bubble.

Reference

Anon., "Photographing a bullet in flight", Conquest magazine, Sep. 510-515 **(1920).**

Beams J. W., "The use of Kerr Cells", Rev. Sci. Instr. 1, 780-93 **(1930).**

Bertolotti M., "Masers and Lasers (an historical approach)" Institute of Physics University Rome **(1983).**

Cranz C., Glatzel B., "Photographic recording of ballistic and other rapid phenomena with the aid of the quenched spark" Phys. Gesell., 14, 525-535 **(1912).**

Earnshaw S., Trans. Roy. Soc. London, 150, 133 **(1860).**

Einstein A., Phys. Z. **18**, 121 **(1917).**

Eskind A. H., Hall G. K., "Index to American photographic collection" 3rd Ed.

Gentry T.P., "Two approaches to the high speed imaging of lithotripsy shockwaves in water," presented at the Association for High-Speed Photography conference in Cambridge, April **(1997).**

Gordon J. P., Zeiger H. J., Townes C. H. Phys. Rev., 95, 282 **(1954).**

Maiman T. H., "Stimulated optical radiation in ruby", Nature, 187, 493-4 **(1960).**

Rankine W. J. M., Trans. Roy. Soc. (London), 160, 277 **(1870).**

Rayleigh J., Proc. Roy. Soc. (London) 84, 247 **(1910).**

Riemann B., "Gesammelte mathematische Werke", Teubner, Leipzig p. 144 **(1876).**

Schawlow A. L. and Townes C. H., "Infrared and optical maser", Physical Rev. **(1958).**

Talbot W. H. F., "On the production of instantaneous photographic images", Phil Mag. (4th series), January, 73-77 **(1852).**

CHAPTER 2

Experimental set-up

2.1 Introduction

The aim of the present research work is to investigate the optical and acoustic nature of the laser generated cavitations bubbles and the optical investigation of the laser peening technique used for producing surface with large residual compressive stress in such applications as aircraft turbine blades.

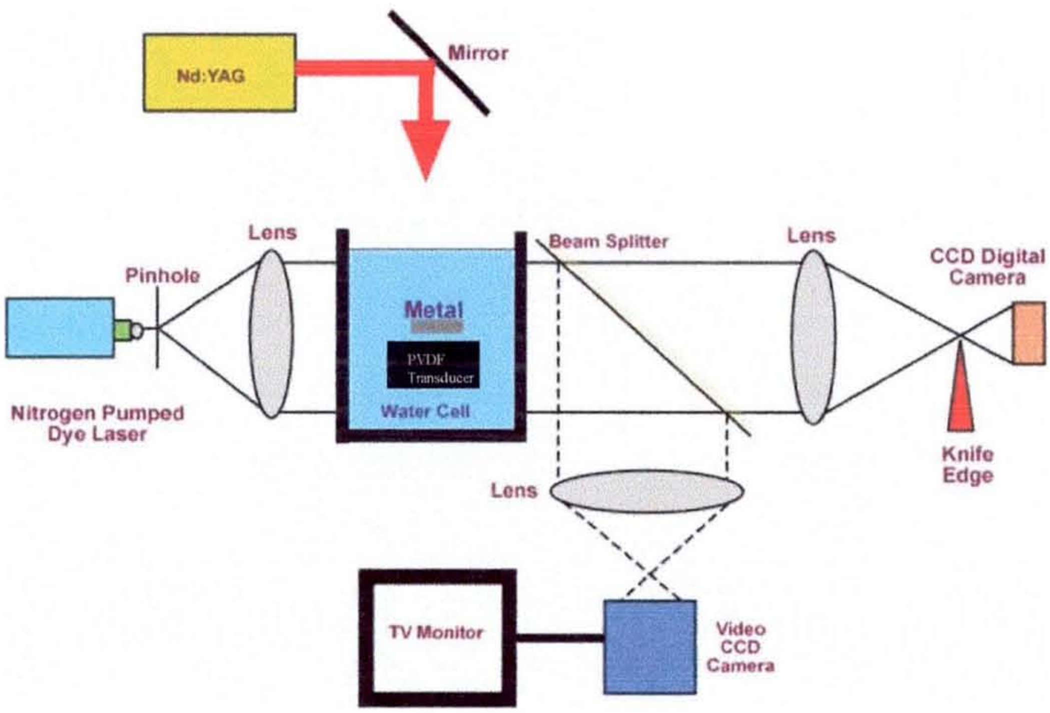

Figure 2.1 Experimental System

The optical system used to carry out the experimentation is shown in figure 2.1. The same experimental set-up has been used to carry out the high-speed study of laser-generated cavitation in liquid and the laser peening process. The cavitation study set-up had a thin film PVDF pressure transducer with a high sampling rate, attached to a digital oscilloscope (LeCroy 350MHz digital Oscilloscope) to observe the shape of the acoustic shock wave produce by the cavity. In the laser peening system, the transducer was replaced by an extra piece of equipment, which acted as a holder to hold the metals that need to be investigated for the peening experiments below the water surface.

The experimental system consists of two main parts. The first part consists of the near infrared Q-switched Nd:YAG laser (emitting a coherent beam of light at a wavelength of 1064nm, with an energy output of about 600mJ and pulse duration of 13ns) which was used to produce the cavitation event and for the metal surface interaction for the laser peening experiments.

The second part of the experimental system is the high-speed image recording system. It comprises a nitrogen pumped dye laser, with a pulse duration of ~0.5ns, which is used as an ultra-fast light source to illuminate the high-speed event in the water. A digital camera with 1.8 MPixel CCD (Minolta RD175) combined with a Schlieren technique to enable visual observation of the acoustic shock waves.

2-2 Cavitation Generation/Laser peening System

The system used to generate the cavitation and to peen metal surfaces made use of:

- Nd:YAG laser beam with a energy output per pulse of ~600mJ, pulse duration of 13ns and a wavelength of 1064nm.
- 35mm camera lens.
- Cell made of two 4mm thick glass plates glued to the outside of a U-Shaped aluminium block.

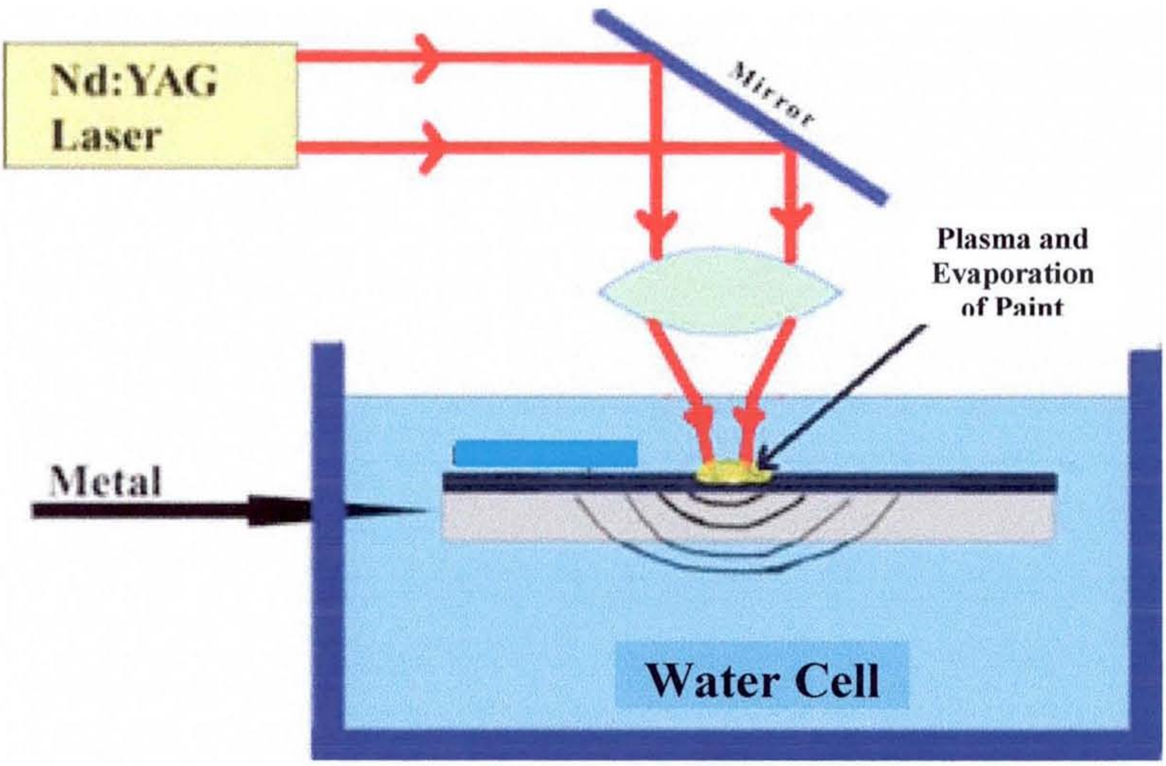

Figure 2.2 Cavitation Generation System.

2-2-1 Beam Focusing

The arrangement is shown in figure 2.2. To achieve the highest laser intensity in water from the laser beam, it must be focused to the smallest spot size possible. To keep the intermediate laser intensity low, the angle at which the beam is focused should be large. Also due to the spherical aberration of the lens a focal line is obtained rather than a focal point from the focusing of the beam. This causes multiple break down in the water, which can be avoided by using a short focal length lens. Figure 2.3 shows examples of poor and good breakdown in water.

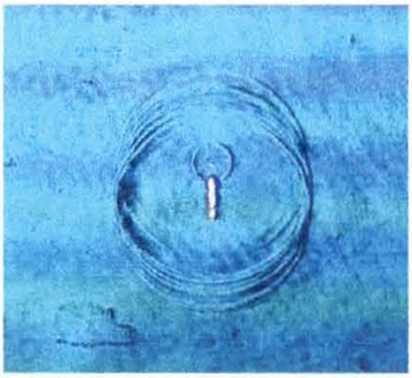

Figure 2.3a multi-breakdown in water

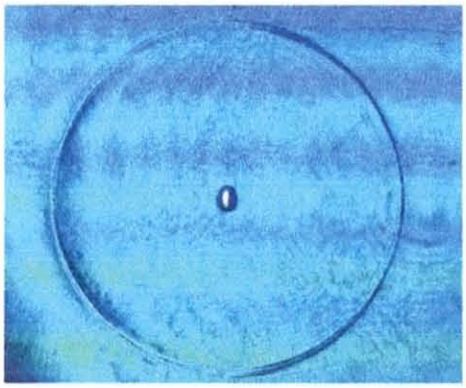

Figure 2.3b Clean breakdown in water with the generation of one plasma.

The Nd: YAG laser is focused in the cell filled with distilled water. The laser beam was first expanded using a biconcave lens and then focused by a 35mm focal length plano-convex lens to produce a spot size of about 10μm in the water. Maximising the cone angle creates the largest possible angle of focus for the final lens into the water, but it should be noticed that this angle in the water due to refraction is smaller than in air. The pressure of the surroundings was constant and could be considered equal to that of air around 101 kPa. The water density and the velocity of the acoustic waves were about 998 kg m^3 and 1490 m s^{-1} at a room temperature of around 293K. The focus of the laser beam was achieved at a depth of about 20mm from the surface of the water.

Due to the high energy laser pulse (600mJ), it was found that the focusing lens used to focus the beam tended to degrade with time and needed to be replaced in order to keep a clean focus. The degradation was due to breakdown occurring on flaws or dust on the glass, which resulted in the absorption of energy in the glass, forming a cavity similar to that occurring in the water. A damaged lens is shown below in figure 2.4.

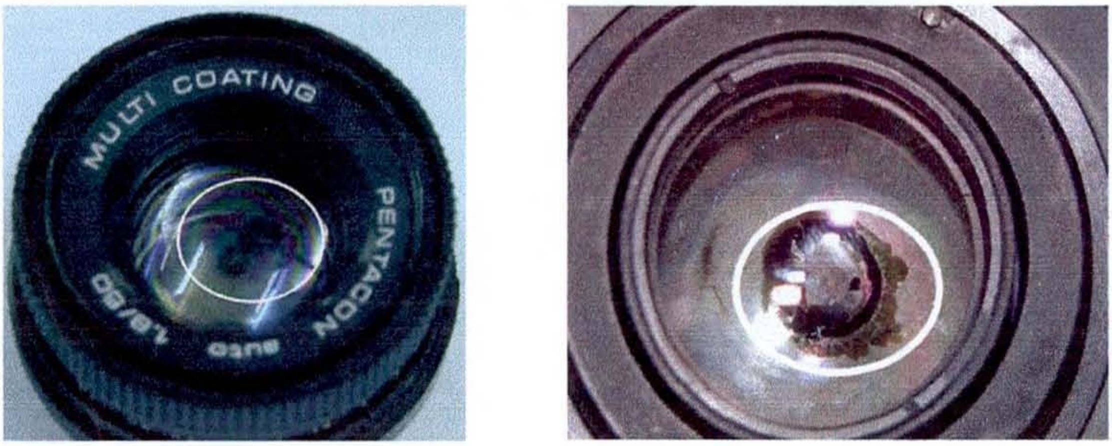

a) **b)**

Figure 2.4 Plano convex lens showing damage due to the passage of high intensity IR laser light energy. **a)** Shows the damage to the multi-coating and **b)** shows breakdown damage within the glass lens.

2-3 The Nd:YAG Laser

The Nd: YAG laser used to generate the cavitation event and for producing metal surface with large residual compressive stress is a Q-Switched Spectron SL450 pulsed Nd: YAG laser system. The laser is composed of a power supply unit and a laser head connected by a flexible umbilical. The laser head comprises the laser oscillator and all other optical components, which are mounted on a series of invar bars, which give the laser mechanical and thermal stability during its operation.

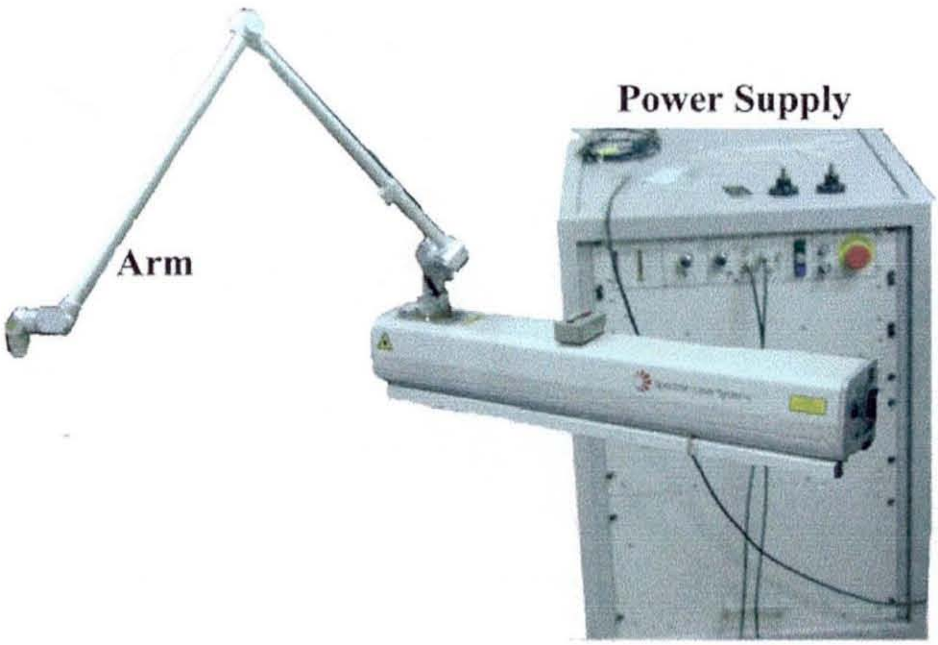

Figure 2.5 The Spectrum Nd:YAG Laser

The neodymium (Nd) laser belongs to the group of the solid state lasers where the active ions are Nd^{3+}. It was first used in 1961 with glass as the host material. Since 1964 Yttrium Aluminium Garnet (YAG) has been used as the host material (Schiffers, 1997).The active medium of an Nd:YAG laser consists of triply ionised neodymium (Nd^{3+}). These ions are an impurity in the cubic crystal of yttrium aluminium garnet with a concentration of 1%. The chemical formulae of YAG is $Y_3Al_5O_{12}$. It is very useful as a laser material because of its excellent thermal conductivity (Hecht, 1992).

The neodymium laser is a four level laser. Its advantage compared to a three level laser is that the lower level is not the ground state of the laser (as is the case of a three level ruby laser). To produce population inversion in a three level laser system at least half of the atoms or molecules have to be raised from the ground state to the upper state which requires very high intense flash lamps as used by Maiman to excite the ruby laser. However, in a four level laser system the lower laser level is only populated by a few atoms i.e. 1%. A population inversion would exist if only about 12% of the atoms could be raised to the upper laser level which is much easier than to excite about half of the atoms to a higher laser level (Hecht, 1988). The essential laser transitions of the Nd:YAG laser are shown in figure 2.6. The most important energy bands corresponding to a pump wavelength of 0.8μm and 0.7 μm. The neodymium ions (Nd^{3+}), excited in the upper energy level, are connected with the metastable upper laser level by fast non-radiative decays. The lifetime of the upper laser level (level 2) is about 244 μsec which is relatively long because of forbidden dipole decay.

The main laser transition is between energy levels 2 and 1. Its wavelength is λ = 1064nm. The population of the lower laser level can be neglected because at room temperature ($E_1 - E_G \approx 10kT$) the Boltzmann factor is very low ($e^{-10} \approx 4.5x10^{-5}$). The non-radiative transition from the absorption bands to the upper laser level, the evacuation of the lower laser level as well as the excess photon energy of the pump photons generate a lot of heat in the crystal. In this case the ten times higher thermal conductivity of the Nd:YAG laser compared to an Nd:Glass is of great advantage (Kneubuhl, 1991).

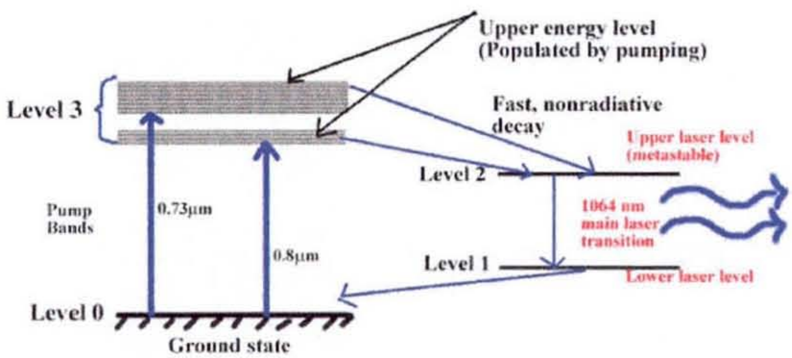

Figure 2.6 Simplified four energy level of the Nd:YAG laser.

2-4 High-speed image recording system

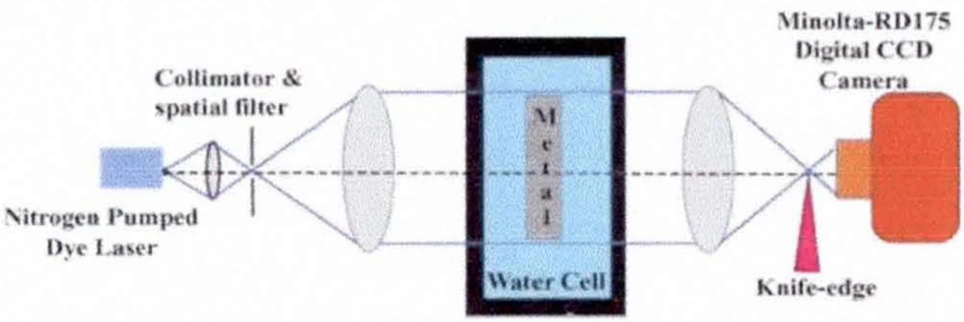

Figure 2.7 High Speed Photographic System

The second part of the experimental set-up shown in figure 2.7 consists of the image recording system, which records the image of the cavitation formed and the peening event. It consists of a nitrogen-pumped dye laser (section 2-5) that is used to illuminate the events, a digital camera (Minolta RD-175) with a 1.8 MPixel CCD (Charged Couple device), combined with a Schlieren technique to enable visual observation of the event.

The Dye Laser supplied a very fast light pulse to illuminate one instant of an event. The coherence length of the laser was 20μm at a tuneable wavelength of 200nm to 1000nm depending on the dye used and used as a control for the intensity of emitted light. The pulse duration was of the order of ~0.5ns, which means no blurring of the final image during the exposure due to the movement of the cavitation or the ablation shockwaves produced during the peening process.

Conventional photography of a stationary object only requires a simple camera to form an image on a film that can later be developed. However, in case of recording an image that travels at the speed of 1500 m s^{-1} (Speed of sound in water) as in the present experiments, the process for recording the image has to be more sophisticated. The pulse of light from the dye laser, which is about 3mm in diameter was expanded and collimated into a parallel beam of about 25mm in diameter before it was used to illuminate the event in the cell. This was done by first focusing the dye laser beam using a 40×microscope objective lens, and then passing the focused light through a 50μm pinhole at the focal point of the objective. The pinhole stops all the light that is non-parallel or diffracted and scattered light due to the defects and dust on the optical components. Therefore the pinhole acts as a spatial filter. The resultant beam, which contains only "Clean" light, is collimated to the parallel beam of 25mm in diameter by a 50mm focal length f/1.7 camera lens. The resultant laser beam is a top hat distribution and proved good light for shadow and Schlieren photography.

When the collimated pulse of dye laser light passes through the event in the cell, the light becomes not "Clean" again due to the refraction, which it goes through. This unclean light is then passed through a 25mm focal length f/2.8 camera lens, and allowed to focus and re-expand. The light then hits the surface of the CCD (Charge Coupled Device) in the digital camera (Minolta RD-175), exposed waiting to record the change in the light due to the effects of the event in the cell.

2-5 The Nitrogen-Dye-Laser System

The evolution of the plasma and propagation of the shock wave occurs in the sub-microsecond time scale, a source of extremely short-duration light pulse was necessary in order to record the events with sufficient temporal resolution (Paisley, 1993). The light source used in this experimental work was a combination of two laser systems. One of which was used to optically pump the other. The first device was a PRA Nitromite model LN103 TEA nitrogen gas laser operating in the near – ultraviolet region of the spectrum. The second device was a PRA Dye Laser model LN102.

The first pulsed dye laser was realised in 1966 (Schafer, 1977). Its application in scientific research proved to be very good because of its unusual flexibility. Some of the advantages of dye lasers are (depending on the dye medium used):

Tuneable output wavelength from the ultraviolet ($\lambda\sim$ 200nm) into the near infrared ($\lambda\sim$ 1000nm).

Frequency-doubling crystals can extend the emitted wavelength further into the ultraviolet spectrum.

Production of ultra short pulses (<ns).

So far more than 500 different dyes have been identified, some of which allow continuous laser emission. Dye lasers may be pumped using flash excitation like solid state lasers but because of the inter-band relaxation processes they are easily pumped by narrow spectral line source such as the output from a nitrogen laser.

2-5-1 The Nitrogen Laser

Nitrogen lasers are super-irradiant electrical discharges capable of producing up to several megawatts peak output at high repetition rates (10-500Hz), with short output pulses of 1-40 ns duration. The active medium in a nitrogen laser is nitrogen gas which flows through the laser. A fast high voltage discharge populates the upper laser level with a lifetime of 40 ns. The transition to the lower laser level is a vibronic one and emits a laser wavelength of 337 nm.

Figure 2.8 illustrates a typical nitrogen laser pulse from a low-pressure system. In our case (Atmospheric pressure) the pulse length is less than a nanosecond.

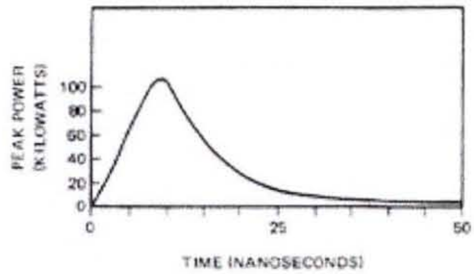

Figure 2.8 Output pulse from a low pressure nitrogen laser

2-5-2 The Dye Laser

The active medium of a dye laser is a fluorescent organic compound which is dissolved in a liquid such as ethanol, methanol or water. The dye molecules are composed of up to 50 atoms which are mostly based on a ring structures and the dye has to be replaced after a certain period of time. The dye used is coumarin.

The energy to drive a dye laser comes from an external source. By the process of excitation, light with a certain wavelength is absorbed in the dye liquid, excites the molecules and loses energy (Stokes shift) which is transferred into heat of the liquid, see figure 2.9. It then fluoresces at another longer wavelength. In this case the dye acts as a wavelength converter.

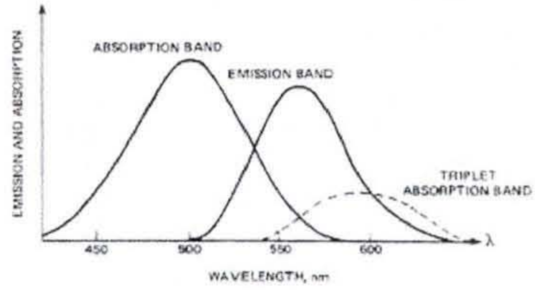

Figure 2.9 Absorption and emission (Fluorescence) spectrum of a typical dye laser.

The typical energy level scheme of a dye laser is shown in figure 2.10. It consists of singlet and triplet states. Laser emission only occurs from singlet states. The triplet states have slightly lower energy than the corresponding singlet states and therefore molecules tend to drop into these states. Because of the long lifetime of triplet states the molecules will be trapped in these states and for that reason they cannot take part in the laser emission process.

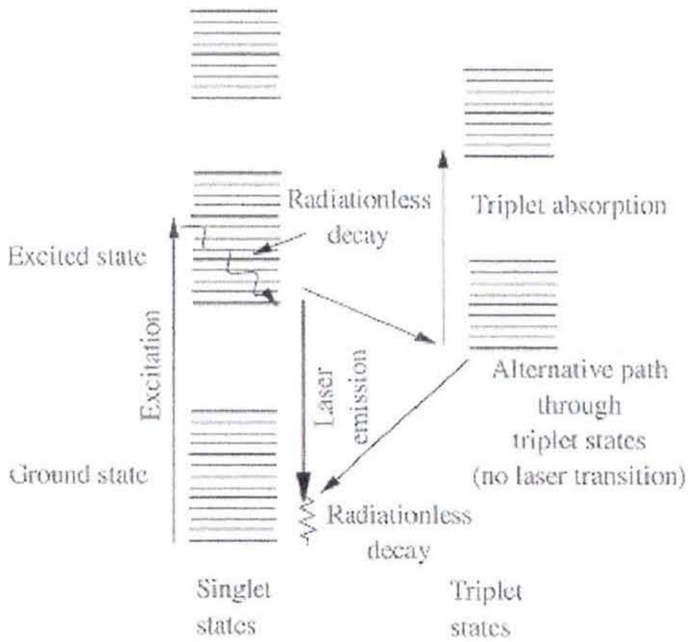

Figure 2.10 Typical energy levels of an organic dye molecule with probable laser transitions, separated in singlet and triplet states. The energy levels (group of lines) consist of vibrational (dark lines) and rotational (light lines) sub-states. Laser transition only occurs from the singlet states.

The optical configuration of the nitrogen pumped dye laser (PRA LN 102 dye laser pumped by a PRA Niromite LN 103 TEA nitrogen laser) which was used to photograph the cavitation bubbles and the peening shock waves in the present experiments is shown in figure 2.11. The pump light from the nitrogen laser with a wavelength of λ=337 nm is focused into the dye cell using a cylindrical lens which pumps a line of dye just inside the front face of the cell. Wavelength selection is provided by the diffraction grating. The nitrogen pumped pulse was about 1ns and the corresponding dye laser reputed to be 400 ps which is short enough to give a high temporal resolution of the event photographed. The dye beam of 2mm diameter with energy of about 15 μJ is emitted via a beam steering prism and an iris diaphragm.

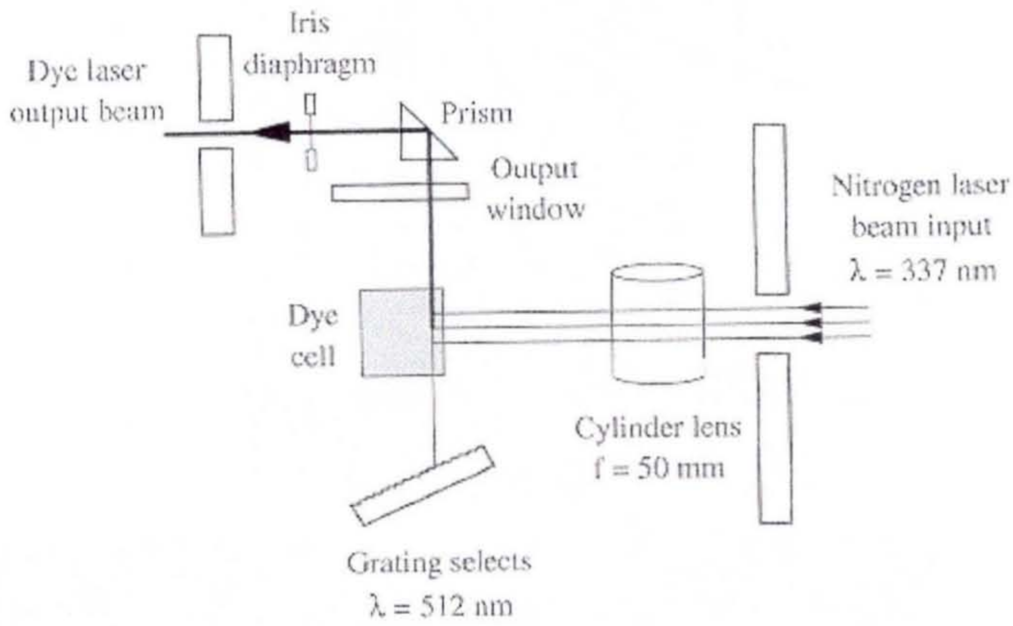

Figure 2.11 Arrangement of the dye and the nitrogen laser with the optical components.

2-6 Schlieren

2-6-1 Introduction

Many problems of science and engineering involve substances that are colourless, transparent and non luminous, so that their observation by direct visual or photographic methods is difficult. However these problems frequently involve changes of the refractive index across the field to be investigated, which can then be visualized or photographed using optical methods that depends on the effects of the refractive index changes on the transmission of light. Interferometer measures the optical thickness (the product of refraction index and path length) whereas Schlieren methods detect the density gradients in a transparent object (Vasil'ev, 1968). Schlieren methods are so called because they were originally used in Germany for the detection of inhomogeneous regions in optical glass, which are often in the form of streaks (Schlieren). Schlieren are those areas in a transparent medium where the value of the refractive index is slightly different from the normal value.

The French astronomer Léon Foucault (1858) first suggested the Schlieren method in 1858 as a means of quality control in the manufacture of large astronomical objectives of high resolving power. In this sense it is known to this day as the Foucault knife-edge method. In 1864, the German physicist, August Töpler (1864), applied this method to the study of gaseous inhomogeneities. In effect, he uncovered a new application of the already known Foucault method, but the great value of the results obtained and the increasingly large role played by gas dynamics in the general development of science have served to attach Töpler's name to this method.

Up to the 20th century, the optical quality tests and the study of gaseous inhomogeneities were the sole area for the application of Schlieren methods. With the advent of the 20th century, Schlieren methods underwent considerable development. They acquired a physical interpretation, based on the laws of wave optics. Rayleigh and Obreimov calculated independently the diffraction distribution of the illumination in the image plane of the Schlieren instrument, working on the assumption that the wave shape in the object plane is a piecewise-linear function of the co-ordinates. A large number of later investigations were based on these fundamental studies, and their importance has increased in recent years, in connection with the development of the diffraction theory of the Schlieren methods.

2-6-2 The Schlieren Technique

The Schlieren effect is observed in everyday life with the naked eye without the need for the experimental set-ups, which are normally used. For example Schlieren is observed above a heater, when rising hot air distorts the background or the heat haze or shimmer on the surface of a hot road in bright light. These are all examples of Schlieren, and the effect is due to the differences in the refractive index of air due to the density variation causing the parallel light to be bent and therefore giving the shimmering effect.

The Schlieren method involves the detection of the laterally displaced rays (due to changes in the density of the propagation medium of the rays as this cause a change to the refractive index) by blocking out or modifying these displaced rays. The blocking or modification can be accomplished by placing a screen in any of the planes of convergence of the light passing through, or being reflected from, the optical region under test. Schlieren photography allows the visualization of density changes and therefore shock waves in fluid flow.

The Schlieren method depends on the deflection of a ray of light from its undisturbed path when it passes through a medium in which there is a component of the gradient of refractive index normal to the ray. It may be shown that the curvature of the ray is proportional to the refractive-index gradient in the direction normal to the ray (Holder, 1965).

A typical Schlieren system is shown in figure 2.12 light rays coming from the slit (or pinhole) are collimated at the first lens, producing a parallel beam of light. The beam then passes a second lens and is brought to focus. If a glass prism is put in the beam path or the test region as shown, it would create an optical disturbance (a deflection). A knife-edge, which is positioned at the focus, cuts off a part of the slit image. An object of constant refractive index change would generate an image on the screen, which is evenly illuminated, and therefore the prism, which generates a refractive index change cause a deflection of the light rays from their original path. These light rays form a bright image on the screen as they are not stopped by the knife-edge. If the refractive index change was in the other direction, the light rays which originally pass through are stopped by the knife-edge as the deflection of light is in the opposite direction, so forming a dark image on the screen or a shadow of the prism. Any optical disturbance due to density change will therefore cause a light deflection resulting in a bright or dark image of the prism on the screen. These results are achieved with a knife-edge, which is sensitive to deflections perpendicular to the light rays and insensitive to deflections parallel to the knife-edge. In our experiment, we can assume the prism as the shockwaves generated, and therefore most of the deflection of light would be perpendicular to the light rays. The knife-edge is therefore placed perpendicular to the direction of travel of the rays in this experimental procedure.

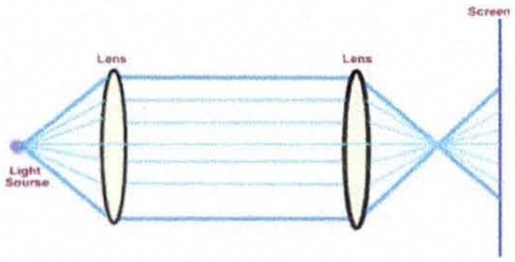

a) Parallel beam of light forming a white circular image on the screen.

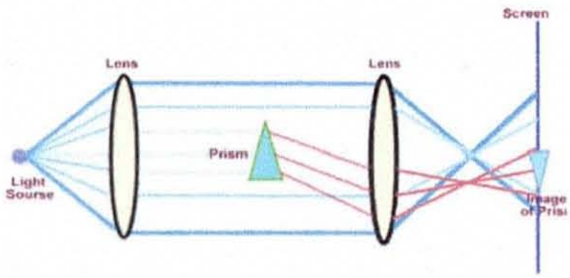

b) placing a prism on the path of the parallel beam will deflect the light and will produce an image of the prism on the screen.

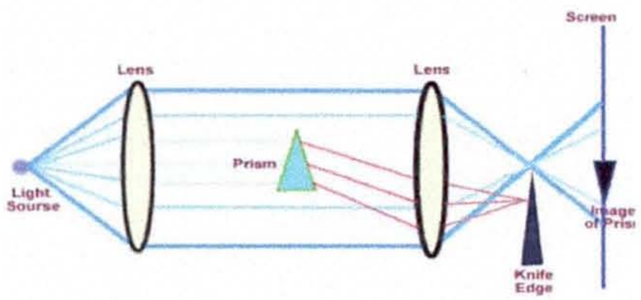

c) the deflected light is stopped by the knife edge causing a shadow of the prism to be formed on the screen

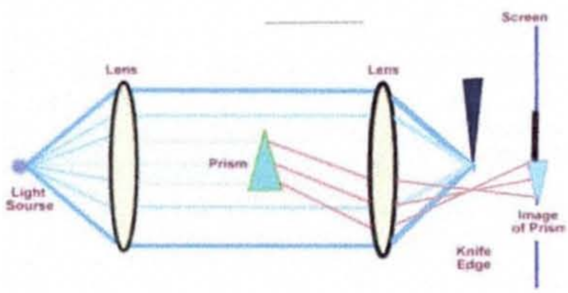

d) the deflected light is not stopped by the knife edge but the parallel beam of light is, so forming a bright image of the prism on the screen

Figure 2.12 The Schlieren Technique.

2-6-3 The positioning of the knife-edge.

The sensitivity of the Schlieren system and hence the visibility of these effects depends on how accurately the knife-edge is positioned in the high speed imaging system. The ideal Schlieren set-up is when the knife-edge is in the focal plane of the lens and obscures exactly half of the area of the Airy disc. In this case every point in the focal spot is made up of elements from the original wave front. Removing half of these elements by the Schlieren knife reduces the intensity of the light across the whole of the final image and a "dimmed" uniform image is obtained. If the knife-edge is moved along the optical axis of the beam, in the direction of the lens or the CCD camera, a diffraction pattern of the knife-edge is obtained. It can be observed as a narrow dark bands running parallel to the knife-edge. Therefore in order to position the knife-edge correctly, to get a good Schlieren effect, it is necessary to move the knife along the optical axis until the image pattern changes to a uniform dim image and not half hemisphere illumination, either on top or bottom due to the knife-edge cutting off half of the beam width. The height of the knife-edge has to be also positioned so that the right amount of light is passing through and just enough of the deflected light is cut off (section 4-4-3).

2-7 Minolta RD-175 Digital Camera.

Figure 2.13 Minolta RD-175

The RD-175 is the first camera to use a beam splitter and three linear charge-coupled device (CCD) targets (two green CCDs and one combination red-and-blue CCD). The primary advantage of this arrangement is that the three medium-resolution CCDs are easier to make and less expensive than a single high-density CCD. The three-way approach also yields better separation of the three colour channels that constitute an image, which virtually eliminates colour aliasing, or imperfectly aligned colours. The three CCD's provide high resolution of 1.75 million pixels (1528x1146). This is achieved through diagonally shifting each CCD pixel to fill any gaps.

The RD-175 uses a 131MB type III PC card hard disk to hold up to 114 images. It produces the largest image files (5MB) and it takes 4.5 seconds to get ready for its next shot. The downside of using a viewfinder condenser is that the RD-175's maximum aperture is f6.7, which allows relatively little light into the camera. It compensates it by using a very light-sensitive CCD which is the equivalent of ASA 800.

2-8 Camera focusing

The digital camera had to be positioned such that it could be removed in order to download the images to a PC and replaced without refocusing. The camera has to be focused at the right position for it to record a clear image of the event occurring in the water tank. The focusing was achieved using a medical needle 0.5mm in diameter. The needle was placed in the water tank, at the point where the Nd:YAG laser is focused, and then the camera was adjusted to the correct position by focusing the needle with white light. The CCD camera was placed in a stand, which allows movement in the forward and backward direction. The needle was used as the focusing object in the plane of the cavitation or peening event due to its relative size and the reflective surface, which is easily seen in white light. It was also used to calibrate the scale of the photos, as the diameter of the needle was known. The size of photographs taken with the CCD camera could be easily calculated by taking a photograph of the needle as a scale.

With a stable set-up of the camera, it was possible to obtain images at different times on the same scale. It was also possible to position the Schlieren knife-edge at the focus and get consistency in the light intensity which depends on the position of the knife edge.

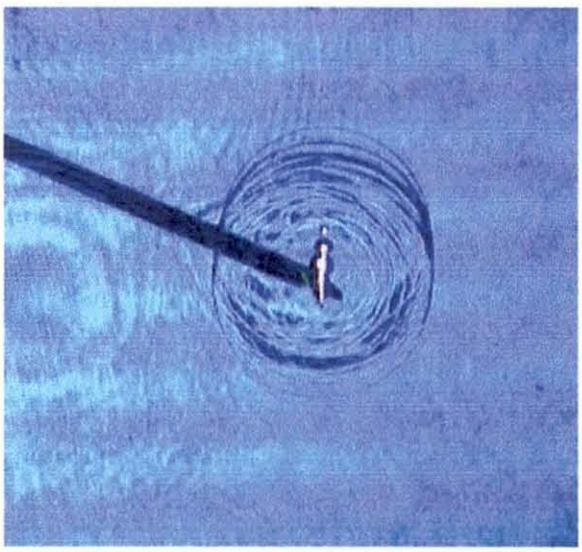

Figure 2.14 Nd:YAG laser beam focused onto the needle.

2-9 The Synchronization of the Experimental set-up

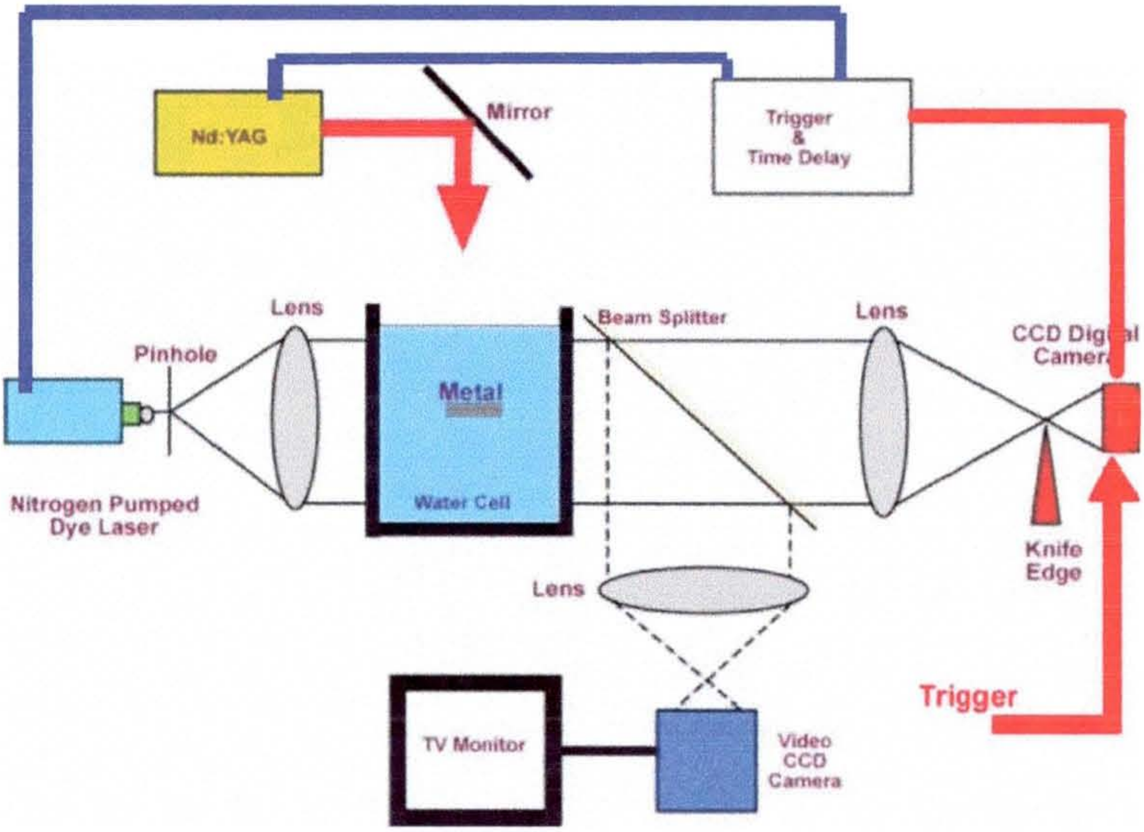

Figure 2.15 The combined function of the experimental system.

The combined operation of the peening system and the high-speed photographic system was achieved using a trigger and time delay box to synchronized the events. The trigger and time delay box was consisted of two signal generators (Lyons Instruments PG 73N Pulse Generator and Farnell 862 Pulse Generator) connected in series to get the desired delays. The signal generators were set to the external trigger mode, with a single pulse output from the generator when it has been trigger with a time delay that can be set. Two signal generators are used so that each laser can be triggered with a signal generator, one for the Nd:YAG laser and one for the nitrogen pumped dye laser.

The system is initiated by a push button, which sends a signal to the Minolta RD-175 camera. This pulse triggers the camera and opens the shutter for a time period of 0.5 seconds; this is a very long period of time compared with the time period for an event to occur in this system.

At the same time, the camera sends a pulse to the trigger and time delay box, which triggers both of the signal generators. The first signal generator sends a pulse to trigger the Nd:YAG laser. The Nd:YAG laser emits a pulse, which get focused into the water tank as explained in section 2-2. The second signal generator also sends a pulse, and triggers the nitrogen pumped dye laser. The pulse send to the dye laser has a time delay set by the signal generator in order for it to illuminate the appropriate time of the event.

2-10 Summary

This chapter described the experimental set-up that has been used in both the cavitations and the laser peening experiment. It gave a brief explanation of each piece of equipment that has been used and the function of it. On the later chapters it will be possible to see how this system was used for each investigation.

References

Charles C. Eagles field " Laser Light – Fundamentals and Optical Communication" St. Martin's Press, (**1967**).

Fiadeiro, P.T. "Wave-front Reconstruction of Optical Disturbances using Digital Image Processing" PHD thesis, December (**1995**).

Gaze Mitchell J. "The effect of Boundary shape on Cavity Collapse of Laser Generated Cavitation Bubbles" MPhys final-year project, (January **2000**).

Hawkes J., Latimer I. ,"Laser Theory and Practice" Prentice hall international series in Optoelectronics, (**1995**).

Hecht J., "Understanding lasers", Howard W. sams & company, (**1988**)

Hecht J., "The laser guidebook", 2nd edition ,Mc Graw-Hill, (**1992**).

Holder D.W. and North R. J., "Schlieren methods", page 4, national physics laboratory, notes on applied science (**1965**).

Kneubuhl F. K., **Sigrist** M. W.," Laser" ,B. G. Teubner, Stuttgart, (**1991**).

Koechner W. "Solid-State Laser Engineering" 5th revised edition, (**1999**).

"**Minolta** Digital Camera RD-175" User Manual.

Orazio Svelto "Principles of Lasers 4th edition" David C. Hanna, (**1998**).

Schiffers Warner Paul "Optical and Acoustic Investigation of Laser Generated Cavitation" PHD Thesis, (October **1997**).

Spectron Laser System, ND:YAG Laser Manual.

Schafer FP ,"Dye Lasers. (Topics in Applied Physics)", Springer-Verlag, Berlin, (**1977**)

Vasil'ev L.A. "Schlieren Methods" Moskva, (**1968**).

CHAPTER 3

Laser Induced Cavitation

3-1 Introduction

The following chapter introduces the reader to the topic of cavitation bubbles and the damage caused by the collapse of a cavity bubble and also how cavitation can be used in a beneficial way. It then goes on to discuss the formation of a cavity bubble in detail, from the optical breakdown in water at the focus of the Nd:YAG laser beam, through to the first collapse and the emission of the shockwave.

In this chapter high speed Schlieren photographs of the oscillation cycle from the formation to the collapse of a cavity bubble are presented. The experimental work presented here was done in order to familiarise the author with the experimental equipment and the high speed photographic technique, so that results obtained could be compared with previously published results. The high-speed photographic system and technique was tested in this experimental work and modified in order to be applied in the later experiments which were carried out on laser shock peening in chapters 4, 5 and 6 which follow.

3-2 What is cavitation?

The word cavitation derives from the Latin word "cavus", which means hollow and means the forming of bubbles of vapour in fluid. The term cavitation can imply anything from the initial formation of bubbles to large scale, attached cavities (super-cavitation). Cavitation arises in a liquid due to a reduction in pressure to some critical value, which in turn is associated with dynamic effects, either in a flowing liquid or in an acoustic field. Any device handling liquids may be subject to cavitation. The extent of cavitation damage can range from a relatively minor amount of pitting after years of service to catastrophic failure in a relatively short period of time. The collapse of cavities can generate very high transient stresses in the vicinity of collapsing bubbles and, if this occurs near a solid surface, can cause material damage and severe wear in a process know as cavitation erosion (Kato, 2001).

Hydraulic machinery such as pumps and turbines are subject to this wear process which increases maintenance cost and decreases service life. It is not usually possible to predict the conditions under which cavitation erosion can occur or its rate, even though this phenomenon has been known for a long time. There is no mathematical model to predict the wear rate of a part subject to cavitation. Lord Rayleigh in 1917 (Rayleigh, 1917) modelled the growth and collapse of a single bubble subject to variation in pressure. Since then researches have addressed this problem with different degrees of complexity and now models can predict with reasonable confidence the dynamics of a collapsing bubble. Cavitation damage, however, is not due to the collapse of a single bubble but rather a collapse of a cluster of bubbles. These clusters can collapse in a way that is much more damaging than the collapse of a single bubble.

The physics of cavitation damage is a complex problem. At the heart of the problem is the impulsive pressures created by the liquid flow around collapsing bubbles. Recent numerical techniques permit detailed examination of the collapse of the individual bubbles (Blake and Gibson 1987). This work has been accompanied by a wide variety of experimental studies (Lauterborn and Bolle 1975, Tomita and Shima 1986, Vogel et al 1989). All of these studies indicate that the final stage of bubble collapse results in the formation of a micro jet that can be highly erosive (Gaze, 2000) as can be seen in figure 3.1. The collapse pressure has been estimated to be greater than 1500 atmospheres in some circumstances (Lauterborn, 1975).

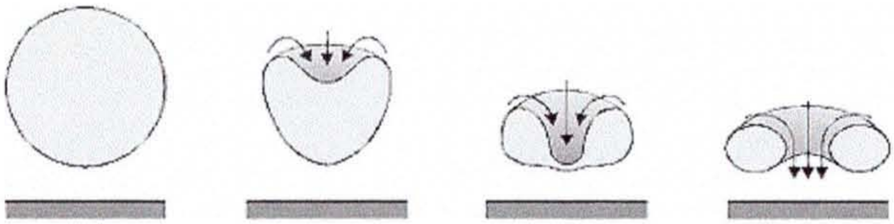

Figure 3.1 During the collapse, a stream of liquid through the bubble is formed. These so called Micro Jets with a diameter of 10 - 100 μm may reach a velocity up to 200 m/s

The actual visualisation of the jet to confirm these theories has proven very difficult, the main problem is to 'look' into a small spherical bubble. Lauterborn (1975) has shown in a sequence of photos how the jet distorts the side of the bubble near the solid.

In practical problems, the combined collapse of a cloud of bubbles is an important mechanism. Hansson and Mørch (1980) suggested an energy-transfer model of intensive collapse of clusters of cavities. Because of mathematical difficulties this problem has not been studied in detail until recently (Prosperetti et al 1993). Earlier work (Wijngaarden, 1964) had already indicated the damage potential of a collapsing cloud of bubbles. Recent work supports this argument (Wang and Brennen, 1994). Very little is known about the correlation between cavitation damage and the properties of a given flow field. It has also been observed that the cavitation pitting rate is measurably reduced with an increased concentration of dissolved gas (Stinebring et al, 1977). An important factor is that the pitting rate scales with a very high power of velocity. Since the velocity in turbo-machinery passages is proportional to the square root of the pressure head, this also implies that the magnitude of the erosion problem is more severe in high head machinery, such as in undersea pumping applications.

Although various materials have different rates of weight loss when subjected to the same cavitation flow, a normalized erosion rate versus time characteristic is often similar for a wide range of materials (Thiruvengadam, 1971).

Many works have been developed in order to gain a better understanding of the cavitation erosion mechanism. From the industrial point of view concerning both machine design and maintenance, the evaluation of the erosion power of cavitation flow and the prediction of the material damage remains a major concern for machinery manufactures and users.

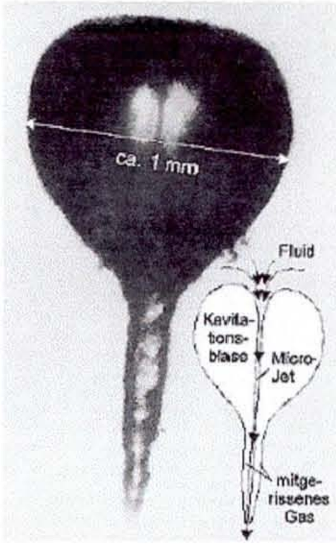

Figure 3.2 Collapsing cavitation bubble with Micro Jet (Vogel, 1989).

3-3 Cavitation Benefits

Cavitation is a word that is perceived negatively by most people and especially by designers of screw propellers and fluid machinery. This is due to the negative effects caused by cavitation, as explained in the previous section due to the high concentration of energy at the collapsing stage of a cavitation bubble having detrimental effects, such as erosion, noise and vibration, on hydraulic machinery. Nevertheless cavitation can also be used for positive proposes such as cutting, cleaning, mixing, improved material strength, agitating chemical reactions, and so forth. Kato (2000) reviewed a wide variety of cavitation applications for practical proposes. These applications extend from the cleaning of a cylinder block of a car engine to the cutting of a human kidney as a surgical knife.

Cavitation can also be used for environmental protection Sato et al (1999) and Kalumuck and Chahine (2000) reported the possibility of using cavitation to decompose chemicals in water. Two other areas of research were "Killing plankton in water using nozzle cavitation" (Kato and Shimomura, 2001) and "Dispersing spilled oil using cavitation jet" (Kato, 2001)

3-4 Cavitation Generation

Cavities are generated in water for two main reasons, one is the reduction in ambient water pressure at constant temperature and the second is a result of local heating of the water or boiling. It is very difficult to study the cavitation phenomena from a cloud of bubbles but if we use a laser beam to produce a localised increase in temperature, this will create a single cavity at an exact location and time. The consequent study of the dynamics of the bubble and secondly fluid flow is then possible.

3-4-1 Optical Break down in Water

The laser radiation interaction process with water is related to plasma-induced ablation and photo disruption, which leads to the emission of shock waves and the growth of a cavity bubble. To achieve optical break down in water that then leads to the formation of cavitation bubbles a number of free electrons need to be generated which starts off an avalanche process.

Water is optically transparent in the visible and the near IR part of the electromagnetic spectrum. A Nd:YAG Q-switched laser will emit laser radiation at a wavelength of 1064 nm, for which the absorption coefficient is 4.35 m^{-1}. When the high intensity laser beam of a Nd:YAG with pulse duration in the nanosecond region is focused in water a two step process to form a plasma begins with molecular absorption. This leads to a very sharp temperature rise with associated ionisation. Due to the thermal ionisation in the focal region electrons are released in a process called thermionic emission. This effect is enhanced by any impurities present in water. However, if the Nd:YAG is in the mode-lock state, pulse duration is typically around 20-30 ps and the dominant initiation mechanism which generates free electrons is called multi-photon ionisation: each photon has an energy quantum of 1.17eV at a wavelength of 1064 nm. To ionise an atom, about 10eV is needed, therefore many photons are absorbed to cause ionisation of the atom. Once the initial breakdown has taken place the plasma grows through an electron avalanche or cascade process: a starting free electron absorbs a photon, it then collides with another atom and ionises it, resulting in one ion and two electrons.

These two free electrons absorb more photons and the whole process is repeated, eventually leading to the formation of plasma. After being formed at the laser focus, the plasma lasts only for a short time which depends on the laser pulse length.

When a Q-switched Nd:YAG laser beam with a pulse duration in the nanosecond region is focused in water, it can generate a power density of about 10^{12} Wcm^{-2} which is high enough to create a plasma in about 10^{-9}s with a temperature of more than 10000 K. A pressure which may be larger than 50MPa is produced (Aitken, and Niemz, 1996). The temperature is attributed to the kinetic energy of the free electrons; due to this the plasma electrons have a high mobility in the plasma medium. The much heavier ions follow the electron movement with a certain time delay. It is the expansion of the mass of the plasma, which stresses the liquid and causes the emission of the shock wave in the surrounding liquid. Studies by Vogel et al (Vogel, 1996) who investigated the shock waves which became detached from the plasma soon after its creation, found that the shock wave may attain a initial speed of about 3000 m s^{-1} which decreases after the first 150 ns to approximately 1500 m s^{-1}. After the acoustic transient is emitted, the pressure in the centre of the plasma decreases and the temperature inside is high enough to vaporise the liquid around the plasma. The vapour is trapped between the plasma and the liquid. As this is a virtually instantaneous process, the pressure of the high temperature vapour increases and is much higher than the outer ambient water pressure, causing the growth of the bubble to release the pressure difference (Schiffers, 1997).

Initially the cavity bubble starts to grow due to the vaporisation of the liquid around the plasma. Work is done against the outer pressure of the surrounding liquid and energy conversion takes place from kinetic energy to potential energy as the bubble expands radially from an initial radius which has the size of the plasma. The speed of expansion of the bubble decreases due to the large liquid mass which has to be expelled in the expansion process. However, despite this reduction in speed, the internal pressure is still higher than the ambient pressure causing the bubble to continue expanding. More fluid is forced to move radially away from the bubble centre, until the bubble reaches its maximum volume where the expansion process ceases and the radius reaches a maximum value. At this point all the kinetic energy is transformed into potential energy. After the bubble passes the equilibrium point, where the surface tension, the viscous force and the static pressure balance the pressure inside the bubble, the outer pressure becomes larger than the inner pressure. At this point, when the bubble has reached is maximum radius, there is a force acting on the bubble's surface towards the centre which starts the contraction process.

Around the bubble's maximum volume, it is difficult to tell when the bubble starts to decrease in volume. Initially when the bubble wall velocity is small the condensation of the bubble's content is sufficiently fast so that the pressure keeps constant. At a later stage of this procedure the vapour/gas mixture of the bubble fails to condense fast enough and therefore becomes compressed as the contraction continues which again leads to a temperature and pressure rise inside the bubble. A further shock wave is then emitted when the bubble reaches a minimum volume due to the highly compressed gas and vapour content of the bubble. The compressed bubble's content together with the inertia of the water acts as a cushion and renders the requirements for an oscillatory system. Figure 3.3 shows this oscillating behaviour of a cavitation bubble for a three rebounds (Schiffers, 1997).

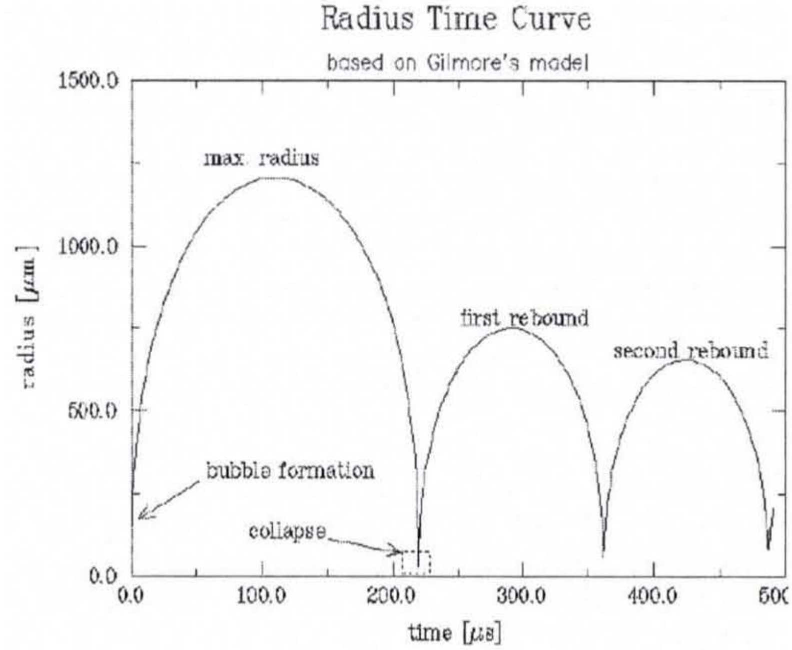

Figure 3.3 Radius time curve for cavitation bubble

Experiments conducted by Vogel and Lauterborn revealed that during spherical bubble collapse a maximum pressure of 6GPa is developed inside a bubble, which reaches a maximum radius of 3.5 mm depending on the laser energy used. They also concluded that the cavitation bubble loses 84% of its energy after the first oscillatory cycle. 73% of this energy, on average, is transformed into the emission of an acoustic transient, which means that the emission of the shock wave is mainly responsible for the strong damping of the bubble oscillation. This can be confirmed from the theoretical work conducted by Ebeling and Fujikawa & Akamatsu (Fujikawa, 1980).

3-5 Cycle of a Cavitation Bubble

The following section describes the motion of the cavitation bubble with a sequence of pictures, which were taken at different delay times between optical break down and the first microseconds after the first collapse. The pictures were taken using the experimental system described in chapter 2. A PVD transducer was placed in the water tank, near where the cavity was formed and connected to a oscilloscope to record the pressure changes in the water. The transducer was fixed on one of the walls of the water tank with a distance of about 2.5cm from the focal point to avoid any interference with the cavitation bubble. The PVD transducer was used to monitor the time between generation and first collapse. Only those events where this is the same were used. The Nd:YAG laser was fired into the water cell, filled with distilled water to produce a plasma followed by the emission of a shockwave and formation of a cavity. The event was recorded using the high speed photographic system described in section chapter 2 sections 2-4.

The series of fifteen images which illustrates the oscillating bubble and the shock waves which are produced at the start of the cavity growth and at the first collapse of the cavity can be seen on figure 3.4. On each image the Nd:YAG laser beam enters from the top to generate an individual cavitation event and the illumination from the dye is achieved from behind, coming out of the paper. The experiment was quite reproducible so that the Schlieren images seen in figure3.4 can be regarded as a sequence of the oscillatory movement of the cavity. In each image, a white dot can be seen, which is due to the self-illumination of the laser generated plasma. Even though the lifetime of the plasma is in the range of few microseconds, it is still visible on a picture taken at 260 μs after the break down. This is due to the long exposure technique used in the high speed photographic system. The system allows the shutter of the CCD to be opened for half a second which, first records an image of the self-illuminating plasma, and secondly of the cavitation bubble which is illuminated by the dye laser a variable time later.

3-5-1 Pictures of the Cycle of a Cavity

a) 0μs

b) 1 μs

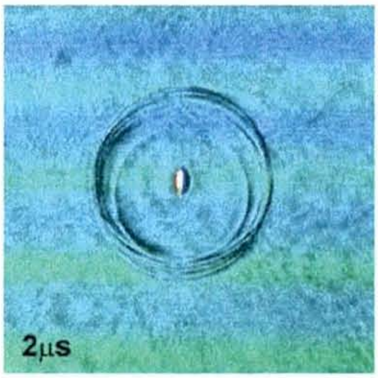

c) 2 μs

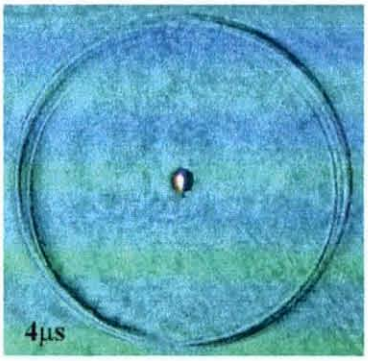

d) 4 μs

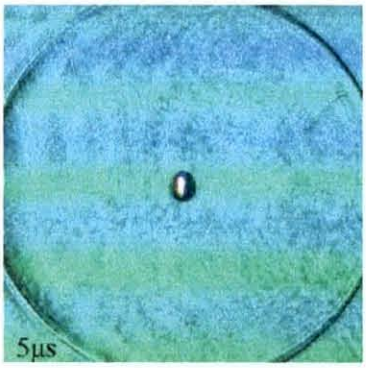

e) 5 μs

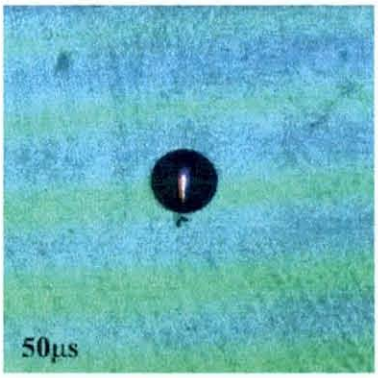

f) 50 μs

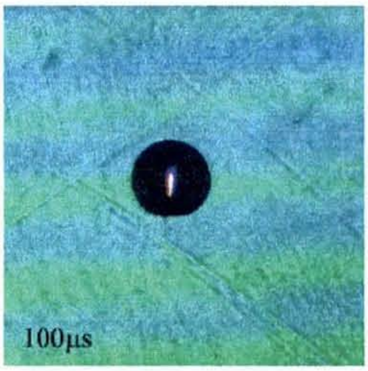

g) 100 μs

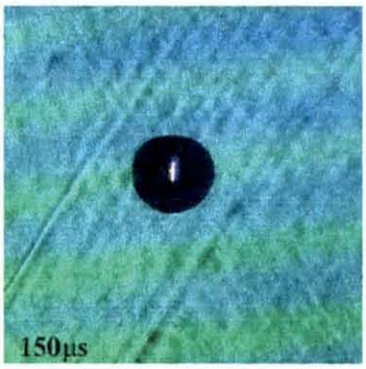

h) 150 μs

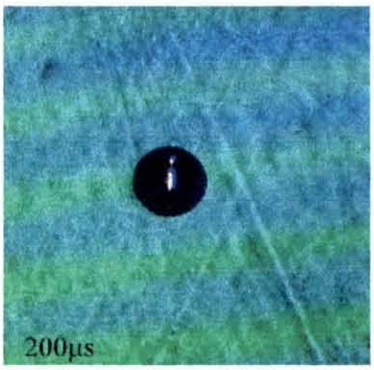

i) 200 μs

Figure 3.4 sequence of images to show the expansion and contraction of a cavity together with the shockwave emissions. Rmax of the cavity is 0.15mm

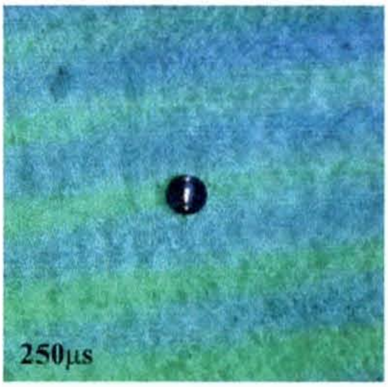

j) 250 μs

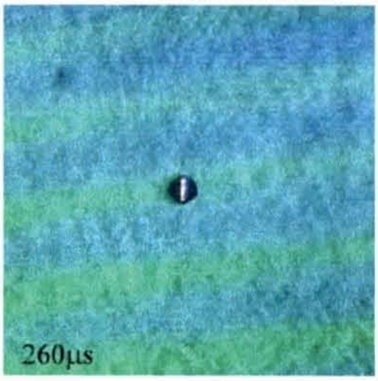

k) 260 μs

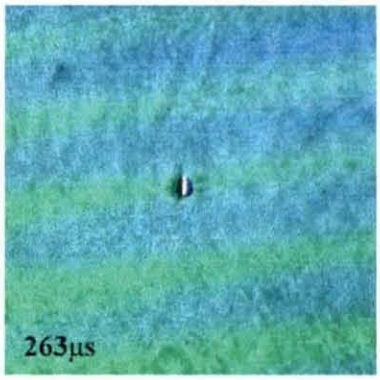

l) 263 μs

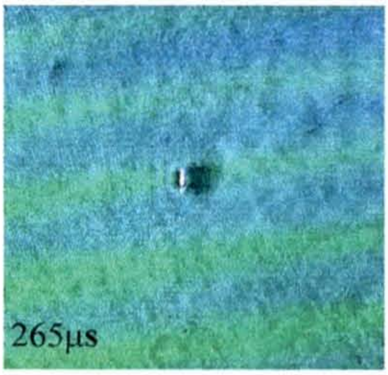

m) 265 μs

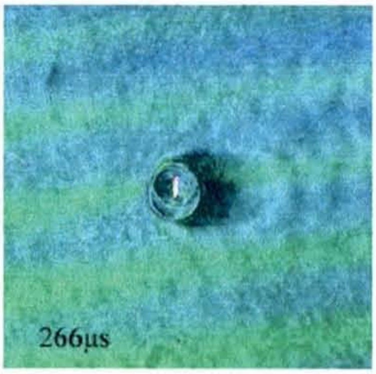

n) 266 μs

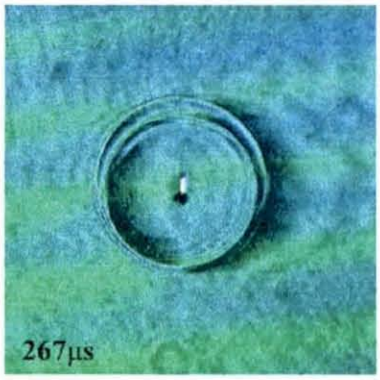

o) 267 μs

Figure 3.4 continued

It is desirable in all cases to generate cavitation bubbles with one plasma source, but in some cases multiple breakdowns at the laser focus were not avoidable as can be seen in figure 4a and 4b due to the variable radiation pattern at the focus. Slightly higher laser pulse energy than indicated leads to a stronger absorption of the laser energy at the impurities around the focal point which causes several plasma dots. Depending on the amount of plasma dots and how close they are to each other, the bubble becomes more or less distorted and loses its sphericity in the early stages (Lauterborn, 1972) this sphericity is recovered on the bubble expansion.

Figure3.4 shows a series of pictures which illustrates the cycle of a cavity bubble from formation to the first collapse. The first five pictures in the sequence, from 0 microseconds delay to 5 microseconds, show the formation of the cavity bubble and the expansion of the initial shock wave. (detail explanation given in optical break down in water section3-4-1) at a time delay of about 4 microseconds (figure 3.4d.) it is already possible to see the cavity bubble has been formed. The bubble will start its expansion process, by doing work against the outer pressure of the surrounding liquid where kinetic energy will be converted to potential energy. This expansion process can be seen for time delays from 5 microseconds to about 100 μs (figure4e). At about 130 μs the cavity bubble reaches its maximum radius Rmax (figure3.5), where the expansion process becomes momentarily stationary and all the kinetic energy is transformed to potential energy. After the bubble passes this stationary point, the outer pressure becomes lager than the inner pressure and the cavity bubble starts to collapse [figure3.4h]. At around 263 μs the bubble reaches its minimum volume and collapses. In this collapse process it emits a shockwave which propagates in the water (figure 3.4m-o)

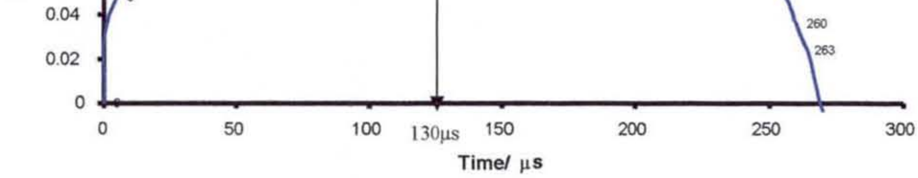

Figure 3.5 Cycle of a Cavitation Bubble. Radius of the bubbles in figure 3.4 as a function of time.

The radius of the cavitation bubble against time was plotted to determine the time period between the maximum radius and the first minimum volume of the cavitation bubble which is the collapse time T_c. The collapse time is half the time between bubble generation and first collapse. An experimental estimate of the collapse time T_c is 265microseconds and the corresponding maximum bubble radius R_{Max} is 0.15mm at 130μs from figure 3.5.

3-6 Detection of the Shock Waves using the Transducer

A focused Q-switched Nd: YAG laser beam with a nanosecond laser pulse generates a power density of about 10^{12} Wcm^{-2} in water, which is high enough to create a plasma in about 10^{-9} s. The temperature of the plasma can exceed 10000K and generate pressures grater than 50MPa (Niemz and Aitken, 1996). The temperature of the plasma is attributed to the high kinetic energy of the free electrons. Due to the high kinetic energy the electrons have a high mobility in the plasma. This movement of mass in the plasma stresses the liquid and causes emission of shockwaves (Aitken, 1996). The cycle of a cavity, or the time from the formation to the first collapse can be deduced, by recording qualitatively the pressure development from the initial laser break down and the first shock wave emission to the first collapse and consecutively the emission of the shock wave. Figure 3.6 shows a pressure profile of a cavity picked up using the transducer and displayed by a Digital Oscilloscope as explained in section 2-1.

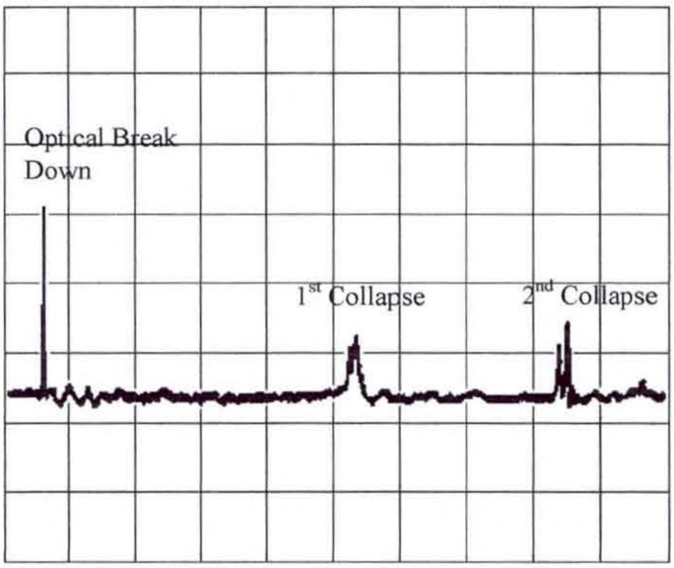

Figure 3.6 Pressure Development of the Oscillating Cavity 50μs/Div.

The oscilloscope has a bandwidth of 350-MHz and a maximum sampling rate of 100MHz, corresponding to 10ns between individual voltage recordings at maximum sample rate. The first peak is due to the shock wave produced by the optical break down. The second peak is due to the shock wave and fluid flow associated with the first collapse.

3-7 Conclusion & Summary

The process of formation and collapse of the cavitation process was explained in this chapter. Visual observation of the process using the high speed imaging system with the Schlieren technique from formation of the plasma to the emission of the first shock wave was carried out; the cavity reaching a maximum radius and then collapsing to emit a further shock wave. The results obtained agree with published results. The maximum radius of the bubble obtained is dependant on the energy delivered by the laser beam to the water, and therefore will have an effect on the collapse time of the cavity.

Comparison with results published (Gaze, 2000 and Schiffers, 1997) matches the result obtained in this chapter, from the emission of the shockwave and the growth of the cavity bubble to the first collapse and further emission of the shockwave. If further investigation of the collapse process was investigated, with longer time delays to observe the second and third collapse, the same effect of emission of shockwave and oscillatory motion of the bubble would be observed, with the maximum radius of the bubble and the strength of the shockwave getting weaker at each collapse as is the case with a mass on a spring due to damping.

a)

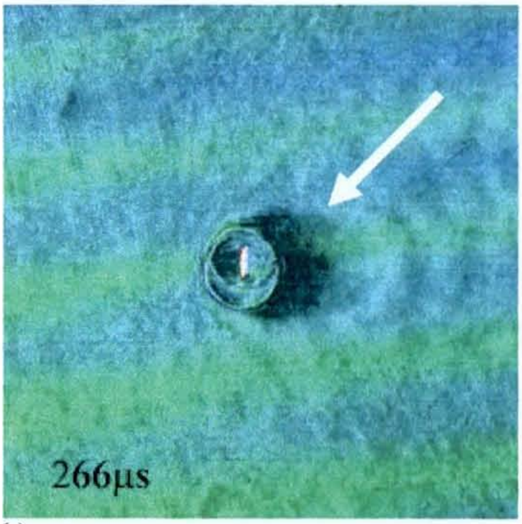

b)

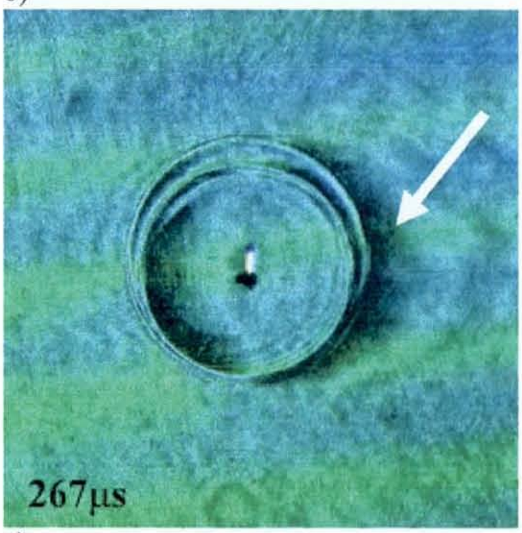

c)

Figure 3.7 m,n and o from the sequence in Figure3.4 to show the Schlieren effect on the pressure gradient around the shock wave.

The pictures shown in figure 3.7 shows the Schlieren effect due to the density changes in the water created by the plasma and the shock waves produced. The three images in figure 3.7 show typical Schlieren images obtained with a knife edge that is positioned vertically, half way through the focal point of the camera lens. This gives the dark area on the pictures as shown by the arrows. The quality of the images depends on the knife edge position and the very sensitive Schlieren image, shows the pressure gradient around the collapsing bubble.

Reference

Aitken F., McCluskey F.M.J., Denat A., "An Energy model for artificially generated bubbles in liquids", J. Fluid Mech (**1996**).

Asshauer T., Rink K., and Delacrétaz G., "Acoustic transient generation by holmium-laser-induced cavitation bubbles", J. Appl. Phys. **76** (9), (**1994**).

Blake J. R. and Gibson D. C., "Cavitation Bubbles near boundaries", Ann. Rev. Fluid Mech. Vol. 19, (**1987**).

Brennen C. E., "Fission of collapsing cavitation bubbles", Fourth International Symposium on Cavitation, California, (**2001**): sessionA5.005.

Chahine G. L., Kalumuck K. M., Cheng J-Y and Frederick G. S., "Validation of Bubble Distribution Measurements of the ABS Acoustic Bubble Spectrometer with High Speed Video Photography", Fourth International Symposium on Cavitation, California, (**2001**): sessionA7.004.

Fortes-Patella R., Challier G., Remound J. L., "Cavitation Erosion Mechanism: Numerical Simulations of The interaction Between Pressure Waves and Solid Boundaries", Fourth International Symposium on Cavitation, California, (**2001**): sessionA3.006.

Fujikawa, S., and Akamatsu, T., "Effects of Non-Equilibrium Condensation of Vapour on the Pressure Wave Produced by Collapse of a Bubble in Liquid", *Journal of Fluid Mechanics*, Vol. 97-3, pp.481-512, (**1980**).

Gaze M. J.,"The effect of Boundary shape on Cavity Collapse of Laser Generated Cavitation Bubbles" MPhys final-report, Loughborough University January (**2000**).

Hallander Jan F. E., "The Influence of Stochastic Processes on the Generation of Cavitation Noise from Mutually Interacting Cavities ", Third international symposium on cavitation, (**April 1998**)

Hansson I. and **Mørch** K.A., "The dynamics of cavity clusters in ultrasonic (vibratory) cavitation erosion", J. Appl. Phys. 51, 4651-4658, (**1980**).

Kalumuck K. M. and Chahine G. L.,"The Use of Cavitating Jets to Oxidize Organic Compounds in Water", J. Fluids Eng., ASME, Vol. 122, pp. 465-470 (**2000**).

Kato H. and **Shimomura** Y., "Erosion Intensity Measurements of Cavitating Jet with Various Configurations", Fourth International Symposium on Cavitation, California, (**2001**): sessionA4.002.

Kato H., "Utilisation of Cavitation foe Environmental Protection – Killing Plankton and Dispersing Spilled Oil", Fourth International Symposium on Cavitation, California, (**2001**): sessionA4.005.

Lauterborn W., "High Speed Photography of laser induced breakdown in liquids" Appl. Phys. Lett. 21, 27-29, (**1972**).

Lauterborn W. and Bolle H., "Experimental investigations of cavitation bubble collapse in the neighbourhood of a solid boundary", J. Fluid Mech., Vol. 72 Part 2, (**1975**).

Leighton T. G., "The Acoustic Bubble" Institute of Sound and Vibration Research The University of Southampton, UK: ACADEMIC PRESS LIMITED, (**1994**).

Lertnuwat B., Sugiyama K. and Matsumoto Y., "Modelling of Thermal Behaviour inside a Bubble", Fourth International Symposium on Cavitation, California, (**2001**): sessionB6.002.

Niemz M. H., "Laser tissue interactions, fundamentals and applications" Springer, Heidelberg, (**1996**).

Olgert L. and Lauterborn W., "Investigation of the Counter jet Developed in a Cavitation Bubble that collapses near a rigid boundary", Fourth International Symposium on Cavitation, California, (**2001**): sessionA5.001.

Pei Zhong, Yuefeng Zhou, and Songlin Zhu, "Dynamic of Bubble Oscillation in Constrained Media and Mechanisms of Vessel Rupture in Shock Wave Lithotripsy", Fourth International Symposium on Cavitation, California, (**2001**): sessionA5.005.

Prosperetti A., "The Equation of Bubble Dynamics in a Compressible Liquid", Phys. Fluids, vol. 30, No 11 (**1987**).

Rayleigh Lord., "On the pressure development in a liquid during the collapse of a spherical cavity", Phil. May. **34**, 94-98 (**1917**).

Schiffers W. P. "Optical and Acoustic Investigation of Laser Generated Cavitation" PHD Thesis, Loughborough University, (**October 1997**).

Storey B. D., Lin H. , Szeri A. J. Franklin and Olin W., "Physically Realistic Models of Catastrophic Bubble Collapses", Fourth International Symposium on Cavitation, California, (**2001**): sessionB6.001.

Vogel A., Lauterborn W. and Timm R., "Acoustic Transient Generation by Laser-Produced Cavitation Bubbles near Solid boundary", J. Fluid Mech. (**1989**).

Vogel A., Bush S., Parlitz U., "Shock wave emission and cavitation bubble generation by picoseconds and nanosecond optical breakdown in water", J. Acoust. Soc. Am. 100, 148-165 (**1996**)

Wang Y.-C. and Brennen, C.E. (1994)," Shock wave development in the collapse of a cloud of bubbles", *ASME Cavitation and Multiphase Flow Forum, (*1994**)

CHAPTER 4

The Laser Peening Process

4-1 Introduction

The following chapter introduce two types of peening process. First is Shot peening which has been used for many years and second is laser shock peening which uses the same technique as shot peening, but the process is carried out with a laser pulse treatment. Peening is a very important process in the automotive and aerospace industry in improving the durability of manufactured components. The following sections describe the peening process and the effect created by the laser shock peening. It describes in detail the effect it creates on a piece of metal when applied to it and the change in metal properties. A visual analysis is carried out on the process by taking high speed photographs of the event using the equipment and the procedures described in chapter 2.

4-2 Peening

Peening consist of bombarding a metal surface with media or laser light to cause the material in the surface to yield. It shakes the metal grains into a more relaxed state, where a thin layer on the surface is placed in uniform compression. This compressively stressed "skin" counteracts tensile stresses and effectively blocks the growth of cracks. Peening is used to reduce premature fatigue failure, loss of strength and surface cracks for naming a few. Since fatigue cracks generally begin at surface imperfections, a compressively-stressed peened skin is highly effective in preventing crack formation and growth. The automotive and aerospace industries are the main users of the peening process, although the technique can also be found in other areas, such as the manufacture of surgical implants. Any metallic component subject to fatigue as a result of cycle stress will benefit from the peening process.

4-3 Shot Peening

Dating back to 2700B.C. Man has made metal objects stronger by means of mechanical pre-stressing or hammering the metal. This hammering process known today as shot peening has been refined to the art of directing the shot to a precise area in order to reduce premature failure of metal components by improvements in fatigue strength.

Manufacturers have been treating engine components such as blades, rotors and gears with shot peening to significantly increase their fatigue life. Shot peening is a cold working process in which the surface to be treated is bombarded with small spherical media called shot. Each piece of shot striking the metal acts as a tiny peening hammer, imparting to the surface a small indentation or a dimple (figure 4.2). In order for the dimple to be created, the surface fibres or crystals of the material must be yielded in tension. Below the surface, the fibres try to restore the surface to its original shape, thereby producing below the dimple, a hemisphere of cold-worked material highly stressed in compression.

Overlapping dimples develop a uniform layer of residual compressive stress in the metal. It is well known that cracks will not initiate or propagate in a compressively stressed zone. Since nearly all fatigue and stress corrosion failures originate at the surface of a part, compressive stresses induced by shot peening provide considerable increases in part life. The maximum compressive residual stress produced at or under the surface of a part by shot peening is at least as great as one half the yield strength (Fairand, 1978) of the material being peened. Many materials will also increase in surface hardness due to the cold working effect of shot peening.

Benefits obtained by shot peening are the result of the effect of the compressive stress and the cold working induced. Compressive stresses are beneficial in increasing resistance to fatigue failures, corrosion fatigue, stress corrosion cracking, hydrogen assisted cracking, fretting, galling and erosion caused by Cavitation (Lindau, 2001) (Further detail on chapter 3). Benefits obtained due to cold working include work hardening, inter-granular corrosion resistance, surface texturing, closing of porosity and testing the bond of coatings. Both compressive stresses and cold working effects are used in the application of shot peening in forming metal parts.

Figure 4.1 shows the process of the shot peening, with a graphical image of the area which is affected by the process and the distribution of the energy from the impact of the shot. Figure 4.2 shows the compression as a function of depth of the metal after one strike of a shot. It can be seen that the most affected area in the metal is the surface, where there is a greater compression. The intensity of the compression gets less as a function of depth. Most of the kinetic energy from the shot is lost at the surface of the metal.

The main purpose of the shot peening process is to:

- Change the orientation and shape of the crystalline structure, which induces different textural barriers to arrest the development of cracks.
- Induce compressive residual stresses, which tend to counterbalance any longitudinal tensile stresses applied by a load or a bending movement.

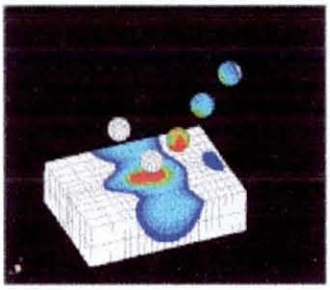

Figure 4.1 Shot Peening with distribution of energy

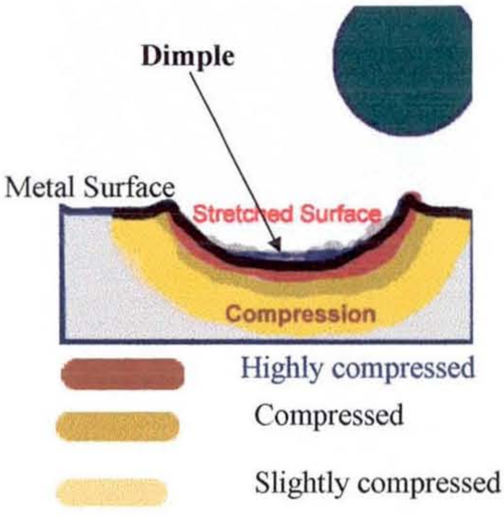

Figure 4.2 Surface Compression

4-4 Laser Shock Peening

The potential of using pulsed laser to generate high intensity stress waves in materials was first recognised and investigated by the early nineteen sixties (Askav'yan, 1963). Laser Shock Peening (LSP) is similar to shot peening as it uses the same technique but instead of using tiny ball bearings to induce residual compressive stress, it uses short duration pulses of light from a high power laser. Laser Shock peening or Laser peening increases the resistance of metals and alloys to fatigue, fretting fatigue and surface cracks by using a high energy pulsed laser to produce residual compressive stresses and strain hardening in the surface of a laser peened part. The residual compressive stresses from laser shock peening extend deeper below the surface than those from shot peening (Clauer, 1996), usually resulting in a greater benefit in fatigue resistance after laser peening. LSP can also be used to locally strain harden thin section of parts.

LSP works by exerting a mechanical force on the treated surface, and the surface is not affected thermally. The effects of the mechanical force on the surface itself are minimal. In softer alloys, a very shallow depression occurs, which decreases in depth in harder materials. The depth of the depression can be increased with increasing intensity of treatment. With LSP only the fatigue critical area(s) on a part can be treated, without masking the area around it. This enables localised treatments around holes, and in and along notches, welds and other highly stressed regions. The intensity of the LSP can be easily controlled and monitored, and tailored to the specific service and manufacturing requirements. The flexible nature of the process accommodates a wide range of parts and geometry and sizes.

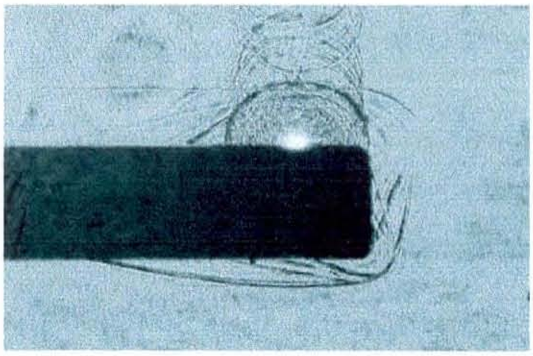

Figure 4.3 Schlieren photograph of the LSP on a piece of steel taken at a delay of 2.5μs.

Figure 4.3 above shows a high speed photograph taken using the Schlieren technique on a piece of steel (Thickness 3.14mm) when treated with the laser shock peening process with a very high energy Nd:YAG laser pulse as can be seen from the intensity of the plasma produced. The high energy intensity was achieved by focusing the laser beam using a powerful lens to increase the explosiveness of the interaction.

4-4-1 The process

Laser shock peening is a mechanical process for treating materials and it is not a thermal process. The laser used is a high-energy, pulsed Neodymium YAG laser, producing a very short pulse, 15 to 30 nanoseconds long and having a wavelength of 1.06 μm with an pulse energy of 50 joules or more (Fairand, 1977).

The schematic of how the process works is shown in figure 4.4. The area to be treated with LSP is covered with two types of overlays, an opaque and a transparent overlay. The opaque overlay can be any material opaque to the laser beam such as paint. Black car paint is used in our case. The transparent overlay can be any material transparent to the laser beam, but liquids prove a more flexible and practical overlay material, so water is mainly used (Fairand, 1977).

When the laser beam is fired and directed onto the surface to be treated, it passes through the transparent overlay and hits the opaque paint (figure 4.4a). It then immediately vaporises a thin surface layer of the paint, which then absorbs the incoming laser energy, rapidly heating and expanding against the surface of the metal and the water. The water layer traps the thermally expanding vapour and plasma against the surface of the metal, causing the pressure to raise much higher than if the water layer was absent (figure 4.4.b). Peak pressures greater than 5 GPa are generated in a metal or alloy when it is covered with a transparent material (Fairand, 1977). The sudden high-pressure against the surface of the metal causes a shock wave to propagate into the metal (figure 4.4c). If the peak stress of this shock wave is above the dynamic yield strength of the metal, the metal yields and plastically deforms.

The stress wave propagates deeper into the metal, and the peak stress of the wave decreases. The deformation of the metal continues until the peak stress falls below the dynamic yield strength. This plastic deformation caused by the shock wave gives rise to strain hardening and compressive residual stresses at the surface of the metal which is one of the most useful effects produced by laser peening (Clauer, 1996).

The main advantage of LSP over conventional shot peening is the relatively large area of the interaction which means that a planar wave is produced. This attenuates more slowly than the point impact of individual shot.

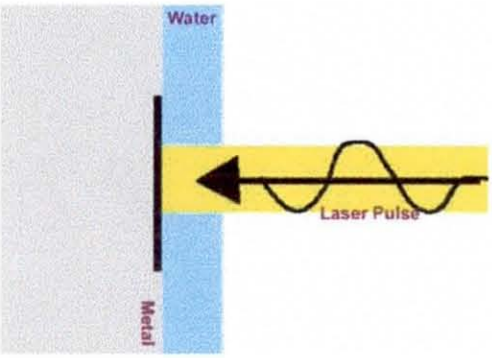

a) The laser beam is focused on the metal surface, which is painted black with a layer of water. The beam passes through the water and strikes the opaque layer or the black paint.

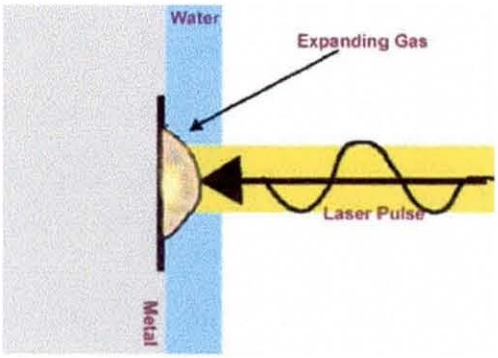

b) It immediately vaporises a thin surface of the paint the vapour then absorbs the incoming laser energy, rapidly heating and expanding against the surface of the metal and the water.

c) The water traps the thermally expanding vapour and plasma against the metal causing the pressure to raise much higher Sudden high-pressures against the metal cause a shock wave to propagate into the metal.

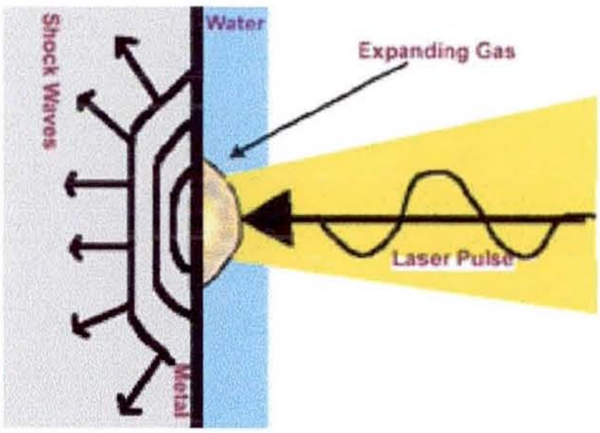

Figure 4.4: Schematic of the Laser Shock Process

4-4-2 Applications of Laser Shock Processing

Many of the potential applications of laser shock processing are based on LSP for increased fatigue resistance and high-value-added parts for improved performance, LSP can also be used to replace a traditional process or material to achieve a cost advantage. Some of the applications that fall into these categories are aircraft engine parts, aircraft structures, medical implants and prostheses, components of power generation turbine and other turbines, specialised gears and parts in valves and other mechanical components having notches, holes and corners prone to fatigue failure.

The laser peen process can strengthen fatigue-prone parts for many applications. Some of the emerging opportunities include:

- Aircraft gas turbine engines
- Aircraft structures
- Land-based gas and steam turbines
- Diesel and gasoline engines
- Automotive and transport vehicles
- Industrial equipment
- Farm equipment
- Medical prostheses
- Tools and dies
- Machine tools and tooling

4-4-3 Shock wave formation and Propagation in the metal/water

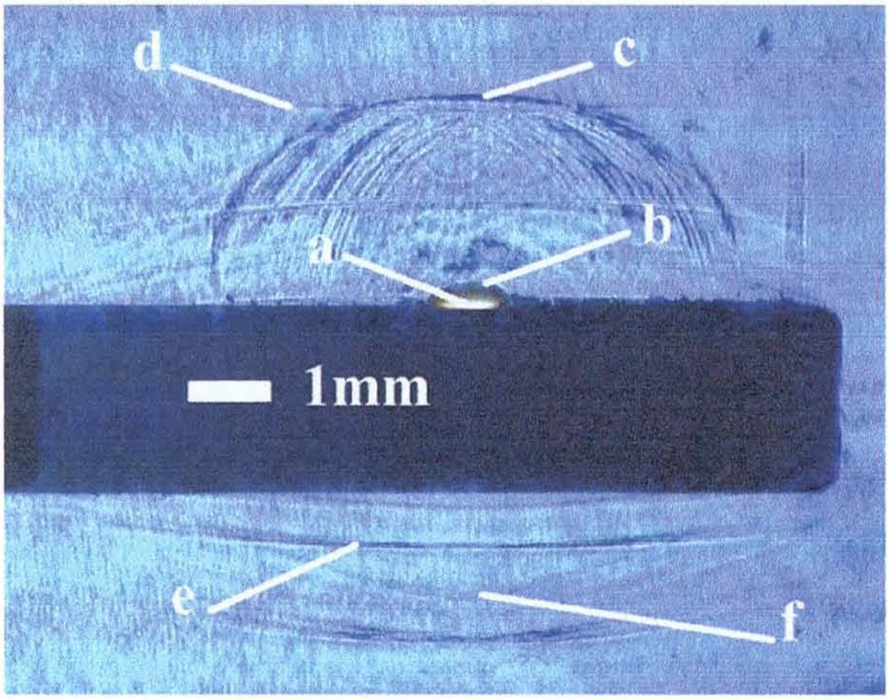

Figure 4.5 A typical photograph taken 2.5μs after the Nd:YAG laser pulse was incident on a 3.2mm thick metal (copper) plate in water.

Explanation of the figure 4.5

a) This is the initial plasma which is generated due to the interaction of the laser beam with the paint below the water (section 4-4-1). The plasma is visible after a certain period of time due to the photographic technique used in the experiment.

b) Shows the vaporised paint, which is expanding due to the absorption of the laser energy.

c) This is the Initial Shock wave- which is produced due to the explosive reaction taking place at the surface of the metal as explained below.

d) The planar shock due to scattered light which is focused onto the metal surface on a larger area but with less effect (Explained in later section "Flat Shock Formation").

e) P wave in steel P-wave in water. Longitudinal waves which are generated due to the interaction of the laser beam with the layer of paint on the surface of the metal.

f) S-wave in steel P-wave in water. The S-wave is converted into a P-wave in the water as S-waves can't travel in water.

The strength of the shock waves seen on the picture is also due to the position of the knife edge as explained in chapter 2 (Section 2-6-3) and shown by the pictures in Figure4.6.

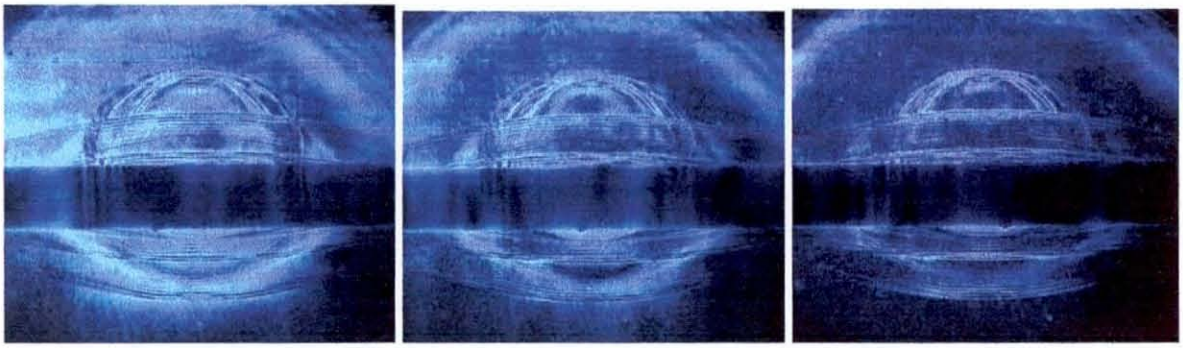

Figure 4.6: The visibility of the shock waves as a function of the knife edge position. The three different pictures have been taken at the same delay with the same piece of metal.

The interaction of the Nd:YAG laser beam with the paint on the metal surface may form a plasma and consecutively generate a shockwave as explained in section 4-4-1. This initial shockwave is circular in shape if a point source but it may be a flatter semicircle if a large area is irradiated (as in the experiment above) although a flat shock is desirable to generate a larger penetration depth. In the initial stage of the process, the cavity and the initial shock wave propagate together in the expansion process with a speed about the same speed as in the water. As the cavity expands and reaches maximum radius, the speed of the expansion reduces due to the opposing water pressure. The shock wave speed decreases and reaches a terminal velocity of 1.5 mm/μs (equal to the velocity of sound in water) in the water and continues its expansion in a nearly spherical shape.

Initial Shock Wave

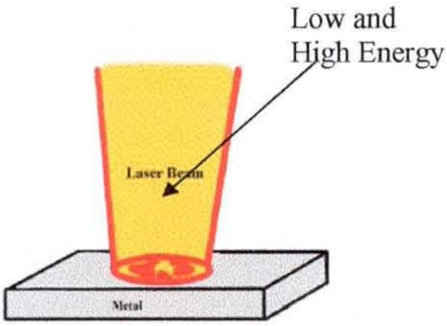

Figure 4.7 illustration of high and low energy regions of the beam delivered by the Nd:YAG laser.

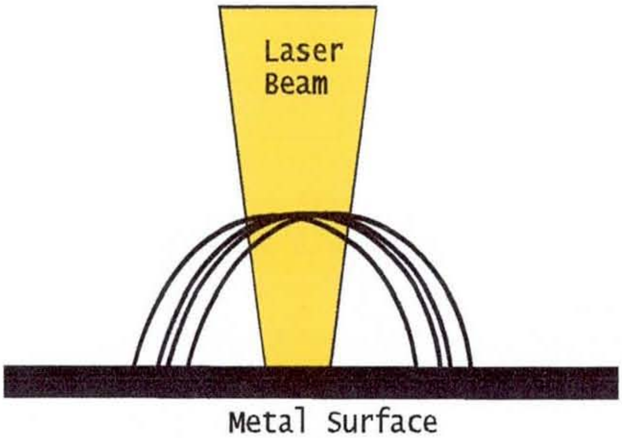

Figure 4.8 The shockwaves produced due to the patchy distribution of the laser beam.

In figure 4.5 it is possible to see many circular shockwaves, which are due to the initial ablation of the paint on the metal surface evaporating in points by absorbing laser radiation and not one circular shock wave as expected. This is due to the non-uniform nature of the laser beam hitting the layer of paint. The radiation delivered from the Nd:YAG laser beam will have patches of high and low energy density regions as shown in figure 4.7. Each of these high density regions will produce a shock wave due to the violent ablation of the absorptive paint layer, which will in return expand in a uniform manner away from the surface of the metal (figure 4.8).

Flat Shock formation

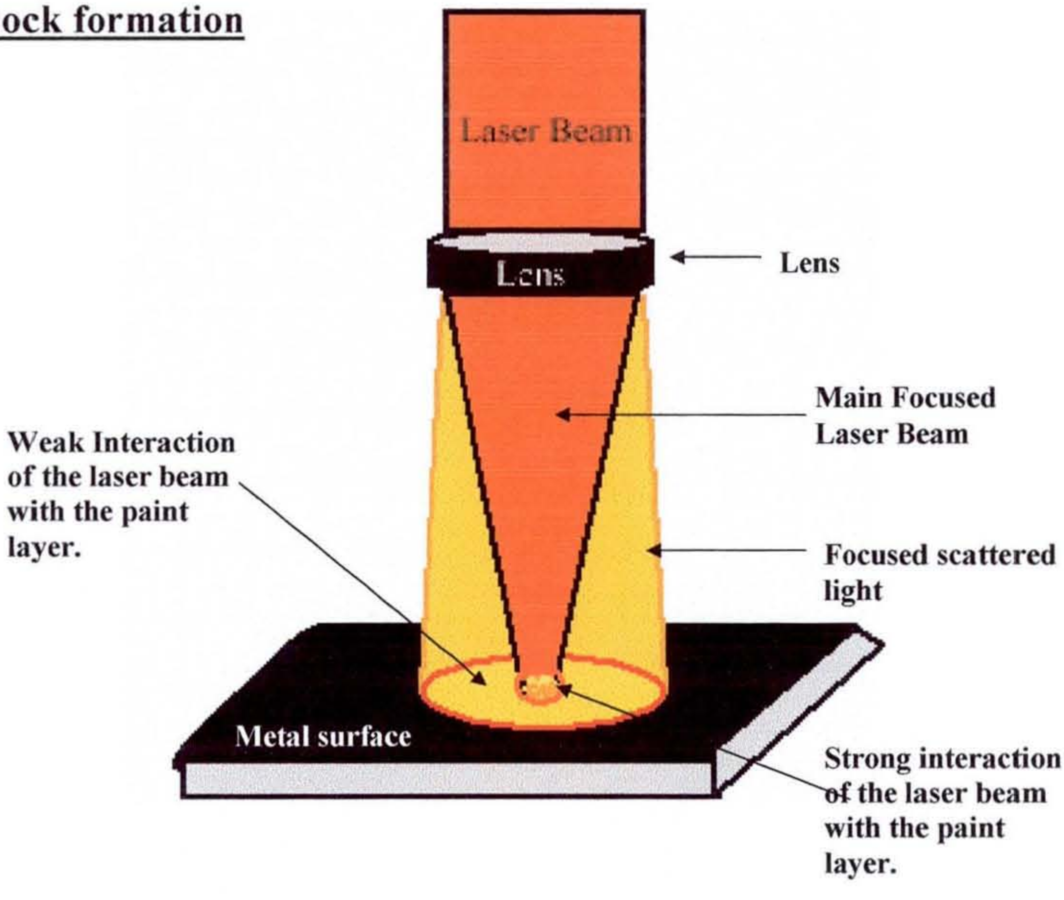

Figure 4.9 The focusing of the scattered laser light to give rise to a flat shock wave.

Figure 4.5 shows a flat shock wave at d which was on the surface of the metal. This flat shock wave in question is situated slightly below the initial circular shockwave. Figure 4.9 shows a schematic of the laser beam focused on the surface of the metal using a lens. The unfocused laser light consists of scattered light due to the flexible arm which is used to deliver the beam from the laser. When this light passes through the lens, the main parallel light is focused on the metal surface as shown in the figure above. The scattered light also is partially focused by the lens in a weak form but it interacts with a larger surface area of the paint than the main focused light. This scattered light is only relatively weak so the large area interaction is rather weak.

The main part of the laser beam interacts with the layer of paint and produces the initial shock wave as explained previously. The weak focus of the scattered light interacts with a larger area of paint, giving rise to the flat shock wave seen in figure 4.5. Its position is slightly below the initial shock wave as it has to cover a greater distance on the same time scale.

S and P waves

There are two types of waves which propagate inside the metal due to the impulse exerted by the laser pulse which interests us: P-waves, or longitudinal waves which are similar to sound waves and S-waves, or shear waves which are transverse waves. The surface interaction also leads to surface waves- Stonley waves and Rayleigh waves. (In figure 4.5 only P and S waves are seen)

P-Waves (or-Longitudinal waves) travel through fluids, and solids. They are compression rarefaction waves and rely on the compressibility and elasticity of the material to propagate. They are sometimes known as "body waves" because they travel through the body of a material in all directions and not just at the surface. For P-waves the motion of the material particles that carry the energy move parallel to the direction of propagation. They travel in the same mechanical way as sound in air. The transmission of the compressional wave is due to the strong inter-atomic forces in the solid.

S-waves depend on the shear elasticity of the material. No shear wave or S-wave can propagate in gases and fluids because gases and fluids have no shear strength. However, the strength of atomic bonds in solids allows them to transmit transverse wave motion.
P-waves are faster than S-waves and in steel they have a speed of 5850m s^{-1} and 3230m s^{-1} respectively as illustrated in Table 4.1. The velocity of the P-waves can be calculated from the elastic constants of materials through which the wave travels as described by the formulae below:

$$V_P = \sqrt{\frac{K + \frac{4}{3}\mu}{\rho}} \tag{4.1}$$

K is the Bulk modulus, μ is the shear Modulus of the material and ρ is the Density.

The velocity of the S-waves is given by:

$$V_S = \sqrt{\frac{\mu}{\rho}} \tag{4.2}$$

Typical wave speeds and related parameters are shown in Table 4.1

		Longitudinal Wave		Shear Wave	
Material	Density ρ (gm/cm^3)	Velocity of Sound ($m\ s^{-1}$)	Acoustic Impedance Z= ρV ($g\ cm^{-2} s^{-1}$)	Velocity of Sound ($m\ s^{-1}$)	Acoustic Impedance Z= ρV ($g\ cm^{-2} s^{-1}$)
Aluminium	**2.7-2.8**	**6,350-6,250**	**$1.69 x10^6$ - $1.78 x10^6$**	**3,100**	**$8.4 x10^5$ - $8.68 x10^5$**
Brass	**8.1**	**4,430**	**$3.59 x10^6$**	**2,120**	**$1.72 x10^6$**
Copper	**8.9**	**4,660**	**$4.15 x10^6$**	**2,260**	**$2.01 x10^6$**
Lead	**11.4**	**2,160**	**$2.46 x10^3$**	**700**	**$0.798 x10^6$**
Steel	**7.8**	**5,850**	**$4.56 x10^6$**	**3,230**	**$2.52 x10^6$**
Stainless Steel	**8.03-7.67**	**5,660-7,390**	**$4.34 x10^6$-$5.93 x10^6$**	**3,120-2,990**	**$2.5 x10^6$-$2.29 x10^6$**
Titanium	**4.54**	**6,100**	**$2.77 x10^6$**	**3,120**	**$1.42 x10^6$**
Water (20°c)	**1.00**	**1,480**	**$1.48 x10^5$**	**----**	**----**

Table 4.1 Typical Wave Speed and Acoustic Impedance Values for Selected Materials

As the Nd:YAG laser beam interacts with the surface of the paint on the metal, it produces the initial shock wave which propagates in the water, away from the surface of the metal, and it also produces an acoustic transient which propagates into the metal. This wave is produced due to the impulse exerted by expanding vaporised paint on the surface of the metal and this wave is responsible for the yielding and plastic deformation of the metal in the peening process. This shock wave propagates into the metal until it reaches the lower metal-water boundary where it is reflected back into the metal and part of the energy is transmitted to the water.

The magnitude of the acoustic wave energy which is transmitted and reflected is governed by the impedances of the two materials (explained in section 4-5). The transmitted wave travels in the water at a speed of 1.5 mm/μs (speed of sound in water) which is slower than the speed of sound in the metal. The reflected wave is inverted by 180° in-phase in the reflection process compared with the original wave (Pain, 1999 and Davis, 1988) and it travels back at the same speed to the upper surface of the metal. When it reaches the metal's upper surface metal-water boundary, the same process which is described above at the bottom surface of the metal plate occurs. The shock wave bounces between the two surfaces inside the metal and transmits some of its energy to the water at each contact with the metal-water boundary. On the lower and upper surface of the metal, wave energy in the metal is released at each reflection at the metal water boundary and hence many "echoes" are obtained in the water.

4-5 Impedance of Sound Waves (Pain, 1999)

If the medium through which waves propagate is lossless, and possesses no resistance or dissipation mechanism, then the acoustic impedance presented by the medium to these waves, as in the case of the transverse waves on the string, is given by the product of the density and the velocity and is governed by the elasticity and inertia of the medium. Although the specific acoustic impedance ρ_0 c, where ρ_0 is the density and c is the speed of sound in the material, is a real quantity for plane sound waves, It has an added reactive component ik/r for spherical waves, where r is the distance travelled by the wave front. This component tends to zero with increasing r as the spherical wave becomes effectively plane.

A longitudinal wave in a medium compresses the medium and distorts it laterally. Because a solid can develop a shear force in any direction, such a lateral distortion is accompanied by a transverse shear.

4-5-1 Reflection and Transmission of Sound Waves at Boundaries

When a sound wave meets a boundary separating two media of different acoustic impedance, two boundary conditions must be met in considering the reflection and transmission of the wave. These two conditions are that the particle velocity and the acoustic excess pressure are both continuous across the boundary.

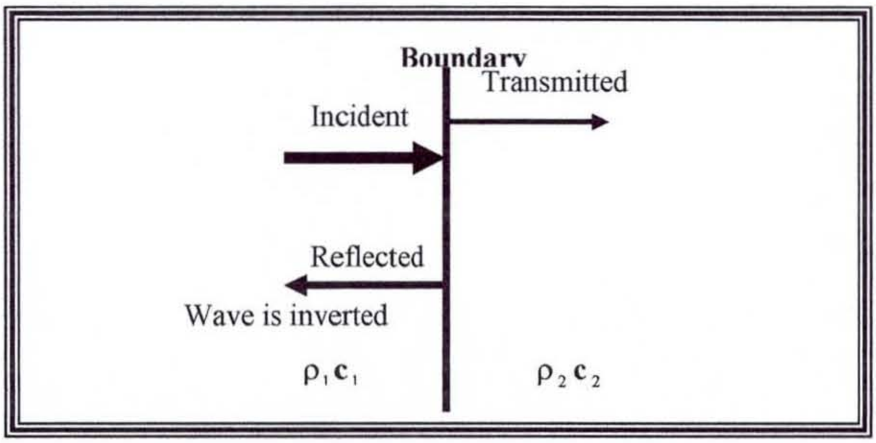

Figure 4.10 Incident reflected and transmitted sound wave at a plane boundary between media of specific acoustic impedances $\rho_1 c_1$ and $\rho_2 c_2$.

Figure 4.10 shows a plane sound wave travelling in a medium of specific acoustic impedance $Z_1 = \rho_1 c_1$ and meeting, at normal incidence, an infinite plane boundary separating the first medium from another of specific acoustic impedance $Z_2 = \rho_2 c_2$. If the subscripts i, r and t denote incident, reflected and transmitted respectively, then the boundary conditions give:

$$\eta_i + \eta_r = \eta_t \qquad (4.3)$$

Where η is the particle velocity

And

$$p_i + p_r = p_t \qquad (4.4)$$

Where p is the excess pressure

Velocity and pressure coefficient of transmission and incident are given by:

$$\frac{\eta_t}{\eta i} = \frac{2Z_1}{Z_1 + Z_2} \quad (4.5) \qquad \text{and} \qquad \frac{\eta_r}{\eta_i} = \frac{Z_1 - Z_2}{Z_1 + Z_2} \quad (4.6)$$

And for the pressure:

$$\frac{p_r}{p_i} = \frac{Z_2 - Z_1}{Z_1 + Z_2} = -\frac{\eta_r}{\eta_i} \quad (4.7) \qquad \text{and} \qquad \frac{p_t}{p_i} = \frac{2Z_2}{Z_1 + Z_2} \quad (4.8)$$

If $Z_1 > Z_2$ the incident and reflected particle velocities are in phase, whilst the incident and reflected acoustic pressures are out of phase. The superposition of incident and reflected velocities, which are in phase, leads to a cancellation of pressure, a pressure node in a standing wave system. If $Z_1 < Z_2$ the pressures are in phase and the velocities are out of phase.

4-5-2 Reflection and Transmission of Sound Intensity

The intensity coefficients of reflection and transmission are given by:

$$\frac{reflected\_Intensity}{Incident\_Intensity} = \left(\frac{Z_1 - Z_2}{Z_1 + Z_2}\right)^2 \tag{4.9}$$

$$\frac{Transmitted\_Intensity}{Incident\_Intensity} = \frac{4Z_1Z_2}{(Z_1 + Z_2)^2} \tag{4.10}$$

Where the conservation of energy would give $\frac{I_r}{I_i} + \frac{I_t}{I_i} = 1$ (4.11)

The large disparity between the specific acoustic impedance of air on the one hand and water or steel on the other leads to an extreme mismatch of impedance when the transmission of acoustic energy between these media is attempted. There is an almost total reflection of sound wave energy at an air-water interface, independent of the side from which the wave approaches the boundary. In the case of water/steel interface only 14% of acoustic energy can be transmitted.

4-6 Conclusion and Summary

The theoretical background to laser peening has been discussed. It is fair to say that the process itself is not completely understood and the actual laser shock processing has only previously discussed from an intuitive point of view. The experiments carried out here were set up and performed to try and confirm or otherwise the shock formation in the laser-paint-metal-water interaction.

The theory of laser shock peening has been discussed in this chapter. Detailed explanation was given of the formation and propagation of the shockwaves in the metal and in the water mediums. It also discussed some of the applications of the peening process and its benefits. The chapters to follow will give experimental results of the laser shock peening process using the high speed photographs and will illustrate the propagation of the shockwaves in the two mediums, metal and water.

Reference

Allan H. Clauer,"Laser Shock Peening for Fatigue Resistance", LSP technologies, Dublin, (**1996**).

Askav'yan G. A. and Moroz E. M., JETP Lett. (1963 R. M. White, J. Appl. Phys. (**1963**))

Atluri S.N., Harris C.E., Hoggard A., Miller N., and Sampath S.G., "Durability of Metal Aircraft Structures", Proceedings of the International Workshop on Structural Integrity of Aging Aeroplanes, Atlanta (**1992**).

Brekhovskikh, Leonid M.,"Waves in layered media", New York ; London: Academic Press, (**1980**).

Davids Norman, "International Symposium on Stress Wave Propagation in Materials" Interscience Publishers Ltd, London, (**1960**).

Davis J. L., "Wave Propagation in Solids and Fluids", New York : Springer-Verlag, (**c1988**).

Fairand B. P., Clauer A. H., R. G. Jung, and B. A. Wilcox, "Quantitative assessment of laser-induced stress waves generated at confined surfaces", Applied Physics Letters, 25(8), 431-433,(**1974**).

Fairand B. P. and Clauer A. H., "Laser Generated Stress Waves: Their Characteristics and their effects to Materials", #50:Laser-solid interactions and laser processing, (**1978**).

Fairand B. P. and Clauer A. H., "Use of Laser Generated Shock to Improve the Properties of Metals and Alloys", Vol. 86-Industrial applications of high power laser technology, (**1977**).

Fairand B. P. and Clauer A. H., "Use of laser generated shocks to improve the properties of metal and alloys", Vol. 86-Industrial application of high power laser tech. (**1977**).

Krasil'nikov, V. A.," Sound and ultrasound waves in air, water and solid bodies", Israel Program for Scientific Translations, (**1963**).

Lindau O. and Lauterborn W., "Investigation of the counter jet development in a cavitation bubble that collapses near a rigid boundary", Fourth International Symposium on Cavitation, California, (**2001**): sessionA5.001.

Nowacki Witold.," Stress waves in non-elastic solids ", translated (from the Polish) by Zbigniew Olesiak, Oxford (etc.),Pergamon, (**1978**).

Pain H. J., "The Physics of Vibrations and Waves" 5th Edition, Imperial College of Science and Technology, London (P 124-127) (**1999**).

Rose Joseph L., Goldberg Barry B., "Basic physics in diagnostic ultrasound" New York: Chichester, (**1979**).

Walters C. T., Clauer A. H., and Campbell B. E., "Laser Shock Effect on Stressed Structural Materials – Experimental Results", Proceedings of the Sixth DOD conference on DEW Vulnerability, Survivability and effects, Gaithersburg MD, (**1987**).

Wasley R.J." Stress wave propagation in solids :an introduction", Dekker,(**1973**).

CHAPTER 5

Shims

5-1 Introduction

This chapter introduces the effect when the laser shock peening pulse is applied to a piece of stainless steel having a thickness of less than 1mm. It discuss the propagation of the shock wave inside the metal taking into consideration the reflections obtained at each metal –water boundary due to the difference in the impedance of the two mediums and the subsequent series of waves in the water.

5-2 Ultrasound

Human hearing can't go beyond about 18,000 vibrations per second, or 18 kHz. There are mammals that can hear well above this. Bats and whales use echolocation that can reach frequencies above 100 kHz. Higher frequencies have a shorter wavelength. A smaller wavelength allows them to reflect from objects with less diffraction and to give greater information about those objects. Extremely high frequencies are difficult to generate and to measure. There may be an upper boundary to usable ultrasound, but scientists have used it up to the 10 gigahertz range.

Generally, the higher frequencies are used for medical imaging, such as investigating a foetus in the mother's womb. The lower frequencies, 1 MHz or less, having longer wavelengths and greater amplitude for a given input energy, produce greater disruption of the medium. The greater disruption leads to increased motion and, in a liquid, the very interesting phenomenon of cavitation. Under the right conditions, irradiation of a liquid with ultrasound leads to the formation and collapse of gas and vapour filled bubbles or cavities in the solution. The collapse of these bubbles can be violent enough to lead to interesting chemical and mechanical effects as explained in chapter 3.

As early as 1822, Daniel Colladen, a Swiss physicist, had used an underwater bell in an attempt to calculate the speed of sound in the waters of Lake Geneva (Holmes, 1974). Other early attempts at mapping the ocean-floor basing on simple echo-sounding methods were nevertheless unrewarding. Lord Rayleigh in England published in 1877 (Rayleigh, 1877) the famous treatise "The Theory of Sound" in which the fundamental physics of sound vibrations (waves); transmission and refraction were clearly delineated. The breakthrough in echo-sounding techniques came when the piezoelectric effect in certain crystals was discovered by Pierre Curie and his brother Jacques Curie in France in 1880 (Richardson, 1962).

Following some early inconclusive experiments relating to the production of electric charge on substances when compressed, the brothers established that crystals which lack a centre of symmetry when compressed along certain axes develop positive and negative charges of magnitude proportional to the applied pressure. Later they discovered the converse effect, a change in the dimensions of the crystal when a potential difference is applied. The name by which this phenomenon is generally known was given to it by Wilhelm Hankel , though some prefer the generic term "piezoelectric effect" (Richardson, 1962).

Ultrasonic waves are also known as stress waves because as they travel they produce a deformation and stress of the surrounding medium. Ultrasonic waves were only studied as a scientific curiosity until the beginning of the 20th century. The main discovery that gave ultrasound a new range of application was the piezoelectric effect. Following the development of the piezoelectric transducer, ultrasound waves were also used by the navy to detect the presence of submerged submarines. Also, during World War II, the military developed ultrasound radar applications. Some of the principles developed at that time lead to the development of SONAR (Sound Navigation and Ranging) (Bolt, 1955) which is the basis of the present diagnostic imaging applications of ultrasound. Ultrasound is currently finding new values and applications in many fields of science, engineering and medicine, such as, detection of defects in materials, industrial and dental drills, ultrasonic cleaning, cardiology and fundamental science such as the study of the molecular properties of materials to mention some of the vast range of applications that can be achieved using ultrasound (Rose, 1979).

5-3 Ultrasound Generation with LSP

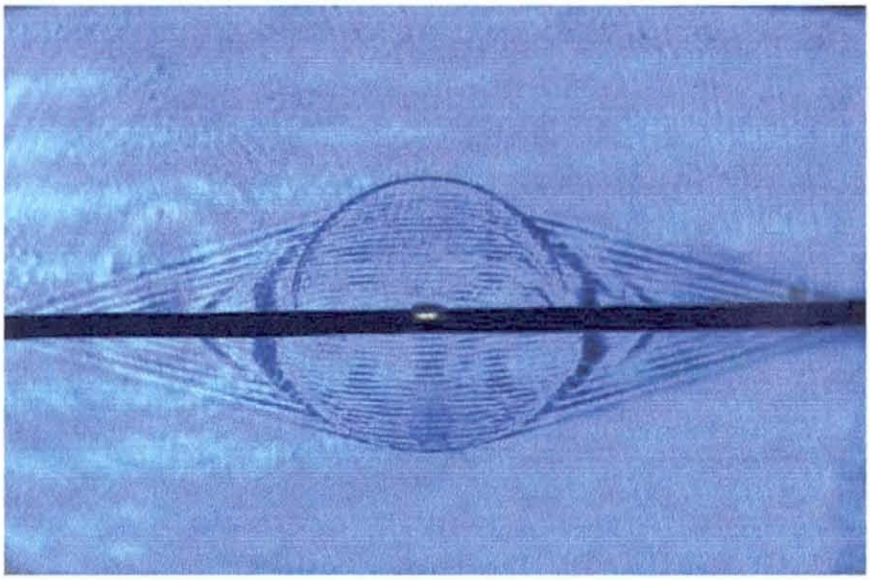

Figure 5.1 High speed photograph of the Laser shock peening applied to a piece of stainless steel 0.7mm thick

5-3-1 Introduction

When the Nd: YAG laser beam is focused into the surface of a metal, coated with a thin layer of paint in water, it creates an ablation shock wave as discussed in chapter 4. This shockwave is due to the violent ablation of the absorptive paint layer and the subsequent plasma, which creates this shockwave in the water, above the metal surface and also gives a corresponding impulse to the metal. This impulse generates a shockwave which propagates into the metal at the speed of sound in the metal and interacts first with the lower surface. After the interaction process with the lower surface, it bounces back to the upper surface, where it interacts with the metal-water boundary again. Wave energy in the metal is released at each reflection at the metal-water boundary and many "echoes" are obtained in the water as can be shown in figure 5.1 above. The distance between the waves which are released into the water is governed by the thickness of the metal and the velocity of sound in the metal. If only the bottom surface is considered, after transmitting some of the energy to the water at the metal-water boundary, the wave has to travel twice the length of the metal before coming back to the lower boundary again to release more energy into the water.

If the impedance sum match between the metal and the water is large then a series of acoustic impulses are realised in to the water at both bottom and top interfaces.

5-3-2 Results

In the following section high speed photographs are shown of the interaction process, when applied to thin pieces of stainless steel or shims having thicknesses of 0.4, 0.7 and 1.27 mm in thickness (figure 5.2, 5.3 and 5.4). Pictures are taken also of the shockwaves generated, with different time delays in order to assess the decay of the wave energy as a function of time as shown in figure 5.5.

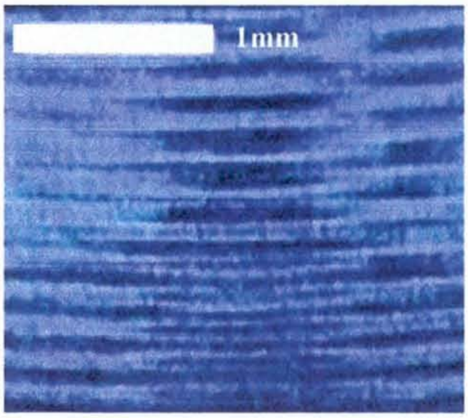

Figure 5.2 fringes created with stainless steel thickness 0.4mm

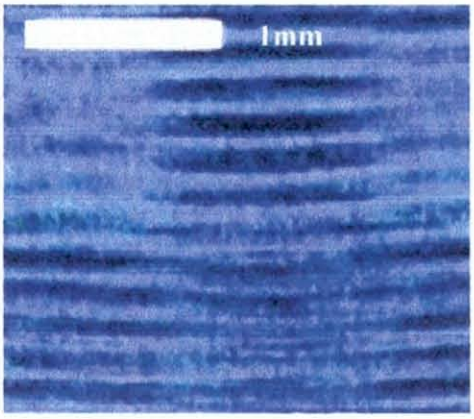

Figure 5.3 fringes created with stainless steel thickness 0.7mm

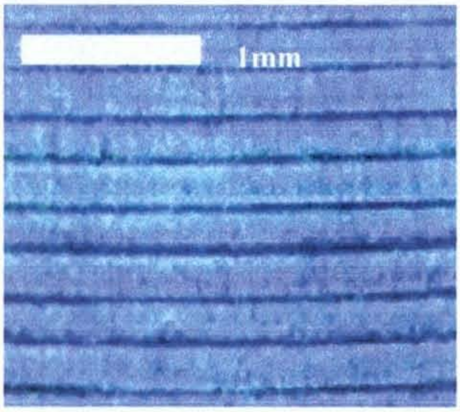

Figure 5.4 fringes created with stainless steel thickness 1.27mm

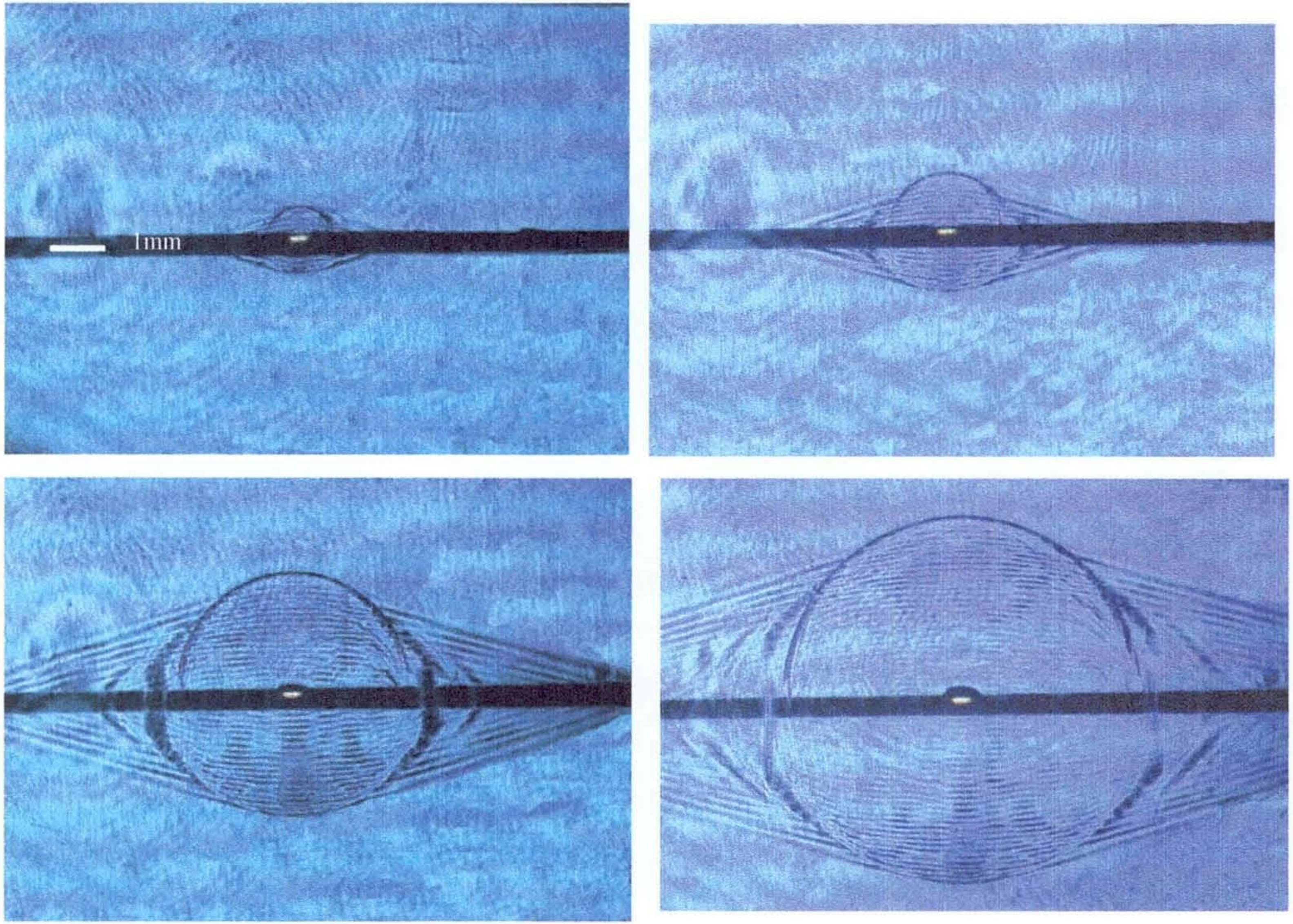

Figure5. 5: LSP on a piece of stainless steel with different time delays. Thickness of the Shim is 0.4mm and pictures are shown at 0.5,1, 2 and 4 μs

The frequency of the ultrasound waves generated is given by f = V_{water}/λ, where $\lambda$the separation of individual waves in water and V_{Water} is the velocity of sound in water. Waves have a frequency of 7.5, 13 and 23 MHz when 1.27mm, 0.7mm and 0.4mm thickness stainless steel is used.

The pressure amplitude transmittance into the water is given by the formulae in $t = \dfrac{2Z_m}{[Z_m + Z_w]}$ where Z_m and Z_w are the acoustic impedance of the metal and water, (section 4-5) where Z_m and Z_w are 46.6×10^6 and 1.5×10^6 kg $m^{-2} s^{-1}$ giving the ratio for transmittance 1.9. In terms of energy only 12% of the incident shockwave energy in the metal is released at each reflection at the metal-water boundary. This wave decay as predicted by the above theory doesn't seem to correlate with the images shown (figure 5.5). The intensity of the waves using the Schlieren image technique, does not appear to decay as quickly as might be thought at first. This is believed to be due to the fact that the darkening is a function of both the refractive index gradient and the Schlieren path length, where the latter increases for longer time delays after the impact.

5-4 Conclusion

This chapter discussed about the theory and properties of ultrasounds and the generation of ultrasound using the Laser Shock Peening process. Further work can be conducted in order to study the emission of the shockwaves when the surface is curved or different shapes can be studied to see the behaviour of the waves.

The ultrasound radiation pattern itself shows interesting features reminiscent of the interference patterns for multiple sources when demonstrating Young's fringes on a water ripple tank (figure5.5). These may be explained by considering the interference between the multiple reflecting waves in the thin plate leading to zones of high and low amplitude on the surfaces of the plate. This behaviour suggests that it may be possible to shape the plate to form a radiating surface, which will result in well-defined ultrasound polar distributions, such as focused or planar waves with possible use in medical ultrasound or ultrasonic imaging.

Reference

Bolt R. H. and Hunter T. F. "Sonics: Techniques for the uses of sound and ultrasound in engineering and science" Wiley, (**1955**).

Don Liyanage D. K. L and D. C. Emmony, "Schlieren images of laser-generated ultrasound" App. Phy. Lett. Volume 79, Number 20 (**2001**)

Holmes J., "Diagnostic ultrasound: Historical perspective", D. L. King(ed), (**1974**).

Joseph L. Rose, Barry B. Goldberg, "Basic physics in diagnostic ultrasound" New York: Chichester, (**1979**).

Rayleigh Lord (Strutt, John William): The theory of sound (MacMillan & Co, London, reprinted by Dover publications, Inc New York) Vol I, p.252, (**1877**).

Richardson E.G. "Ultrasonic physics" Edited by A.E. Brown, Elsevier, (**1962**).

Rozenberg, L. D. "Sources of high intensity ultrasound" Vol1, Plenum, (**1969**).

Williams A. Roy, "Ultrasound: Biological effect and potential hazards" London, Academic, (**1983**).

CHAPTER 6

Ultrasonic Fringes

6-1 Introduction:

When laser shock peening was applied to a piece of copper (thickness =3.14mm) shock waves were generated as explained in section 4-4. In preparation for peening, the metal is made strongly absorbing by being painted black. In some experiments a complicated shock structure was sometimes observed. In the photograph (6.1) the image was taken 2.5microseconds after the firing of the first laser (Nd:YAG) and the exposure time was the usual 400 picoseconds long. Below the primary shock wave were observed ultrasonic fringes or secondary shock waves (figure 6.1), which were not visible in all previous pictures. The area of the metal surface hit by the Nd:YAG laser was about 2mm in diameter. The secondary waves that were generated have a separation of 0.16mm for this particular experiment, which correspond to a frequency of about 9MHz.

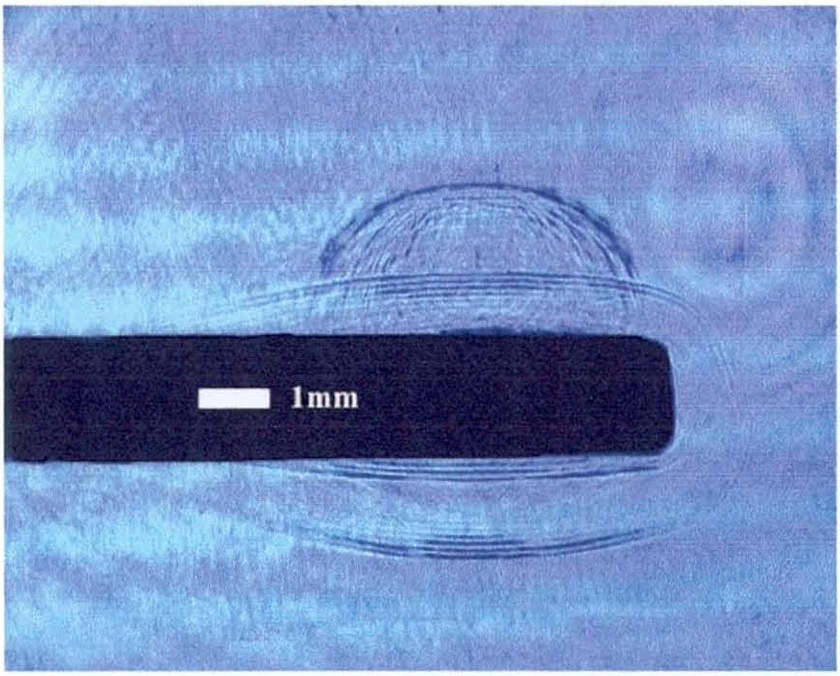

Figure 6.4 LSP on a piece of copper, thickness 3.14mm and time delay 2.5μs.

6-2 Secondary shock waves

The secondary shock waves seen in figure 6.1 are a consequence of the high explosive effect created by the interaction process of the Nd:YAG with the layer of paint. The separation of the secondary waves above the metal and below is the same. This suggests that these waves has been generated at one point in time and then were transmitted and reflected in the same process as the primary waves (more detail on Section 4-4-3). The secondary waves are not visible on the first hemispherical shock wave in the water which is produced due to the explosive evaporation of the paint layer. The waves might be present below the circular shock wave but are not visible due to the number of pressure changes occurring at the start of the event.

The secondary shock waves can be assumed to be generated on the surface of the metal. The secondary shock waves might be caused and partially due to the initial shock wave being trapped inside the paint layer. These shock waves are then transmitted to the metal, which in turn reproduce the secondary shock wave effect at each reflection. The secondary waves are being produced in this case by an oscillation of a very thin section of the metal or the paint layer.

The Schlieren effect of the pressure gradient is seen clearly on figure 6.1. The effect is shown by the dark and white regions above and below the shock waves. The intensity of the dark regions shows the strength of the pressure gradient produced in the water due to the different shock and acoustic waves produced by the explosive interaction of the laser pulse with the paint. From the quality of the dark regions shown by the Schlieren image, it can be assumed that the position of the Schlieren knife is in an ideal position.

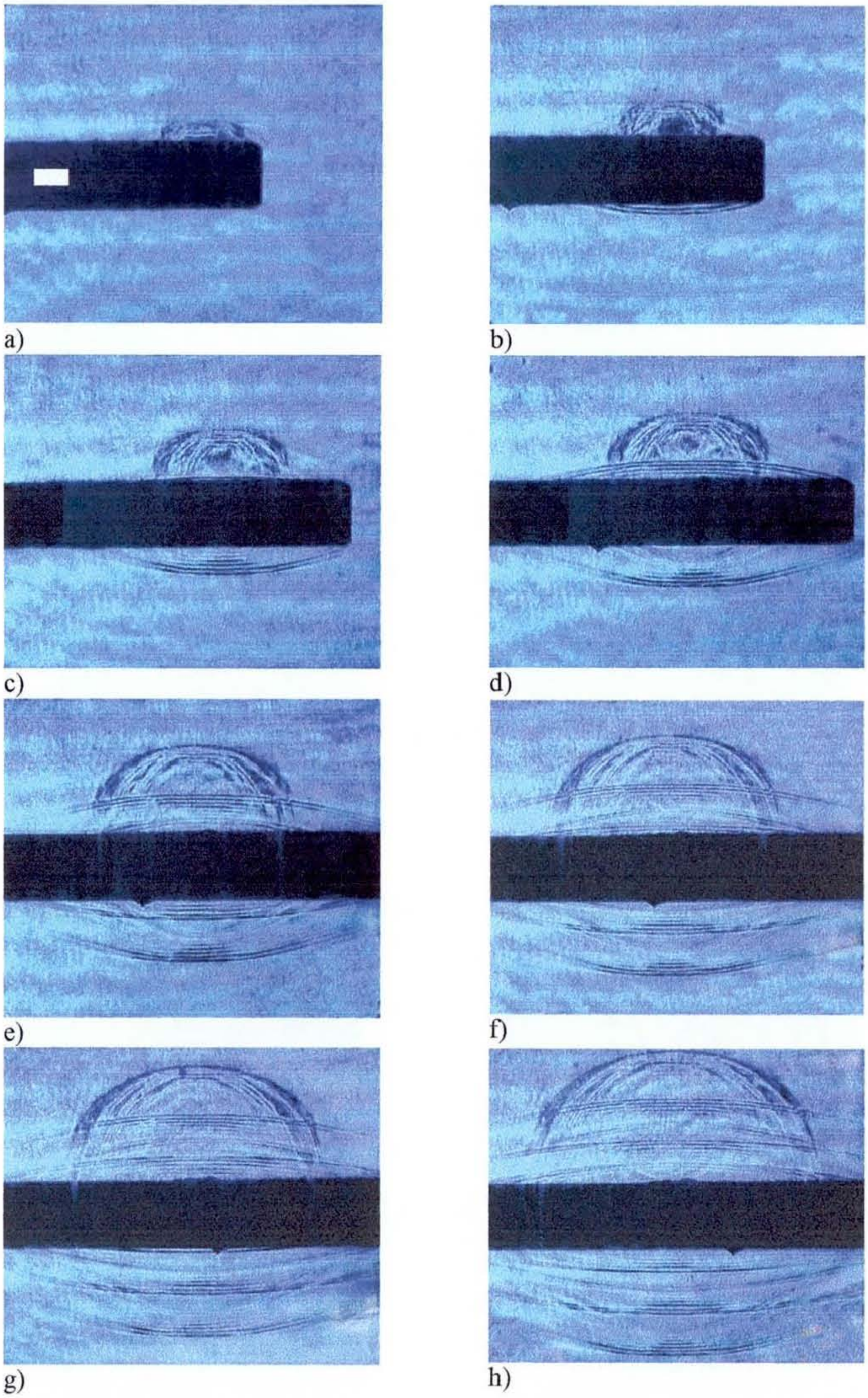

Figure 6.2 A sequence of pictures taken at 0.5 to 4 μs showing the generation of the secondary shock waves. The thickness of the metal is 3.14mm.

Figure 6.2 shows a sequence of Schlieren pictures taken at different time intervals from 0.5 – 4 μs. The metal used in this sequence is the plate of copper used to take picture in figure 6.1, with one layer of paint on the surface. The thickness of the layer of paint used in this sequence is 0.01mm. In figure 6.2, all but **a** (figure 6.2 b-h) show this phenomenon of the secondary waves. The first of the pictures doesn't show this effect as the time delay is too short for the effect to be seen and also there are too many events, due to individual ablation points, taking place in order for the secondary waves to be visible. The intensity of the secondary waves is stronger on the centre part of the picture, where many fringes can be seen.

Figure 6.3 shows an enlarged section from figure 6.2b in the sequence. This picture show a very high refractive index gradient at the centre above the surface of the metal as can been seen from the dark area. This high pressure gradient in the water is due to the expansion of the layer of paint after interaction by the Nd:YAG laser beam. This high pressure region expands and diffuses with time as shown in the sequence of pictures in figure 6.2.

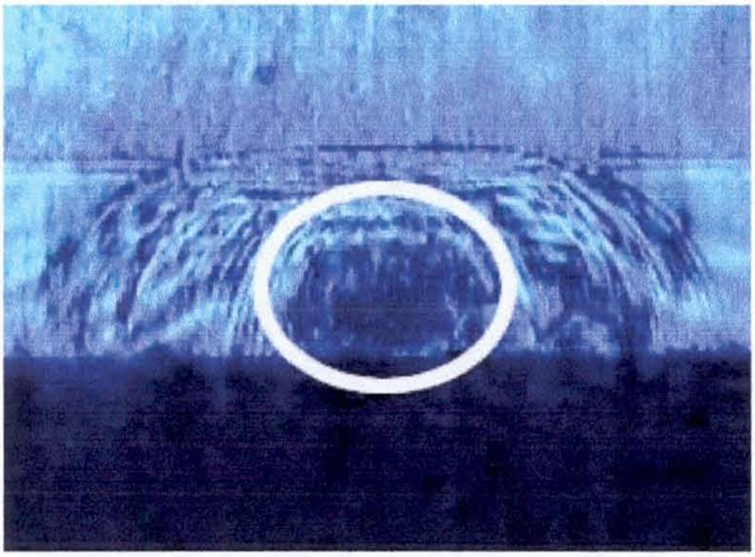

Figure 6.3 Enlarged section from figure 6.2b. The circled area shows the pressure wave front.

6-3 The Effect of Paint Thickness.

In order to try and find an explanation for the fringes, the effect of paint thickness on the separation of the high frequency secondary shock waves obtained was investigated with copper and stainless steel. Laser shock peening was carried out on the surface of the two metals with one and two layers of paint, which were applied as before but with a second coat being sprayed after the first was dry.

6-3-1 Copper

Figure 6.4 shows the results obtained for copper. The results shown for the single and double layer of paint was obtained from two different experiments. This was due to the fact that when one layer of paint was used on a similar piece of copper as with the two layers, no secondary shock waves were visible.

The thickness of the metal used for one layer of paint was 3.14mm and the two layers were used on a metal thickness of 4.47mm. Other variables such as the Nd: YAG laser beam intensity, the wavelength of the nitrogen dye and the position of the Schlieren knife were kept constant. The comparison of the pictures in figure 6.4 **a** and **b** shows that with one layer of paint on the surface of the metal give a bigger secondary shock wave separation than with two layers of paint. This leads to conclusion that the generation of the secondary shock waves is due to the paint layer and not to the metal surface.

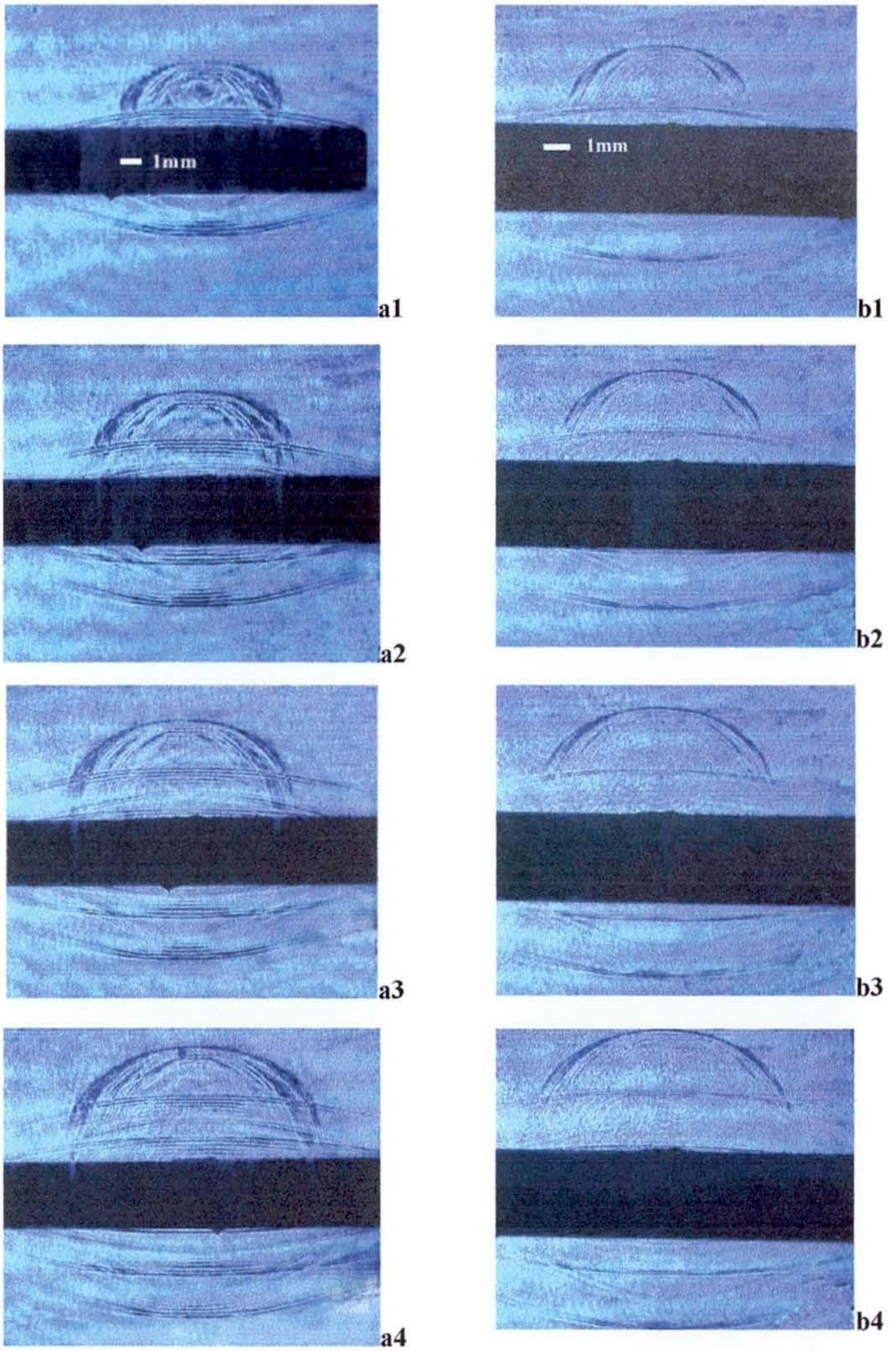

Figure 6.4 Series **a** shows piece of copper (thickness 3.14mm) with one layer of paint. Series **b** shows piece of copper (thickness 4.47mm) with two layers of paint on the surface. *The fringe separation is shown enlarged in figure 6.6.*

6-3-2 Stainless Steel

The same experiment as with copper was carried out with stainless steel. Figure 6.5 shows the effect when laser shock peening is applied to a piece of stainless steel. Figure 6.5 **a** show the generation of the primary and secondary shock waves with one layer of paint and figure 6.5 **b** show the same process when two layers of paint is applied to the surface of a different piece of stainless steel. When one layer of paint is used on the surface of the metal to make it strongly absorbing to the laser radiation the separation of the secondary shock waves obtained is large compared to when two layers of paint is applied to the surface, but in the second case the fringes are barely visible.

As in the case with copper, the metal thickness used for the one layer of paint is 3.14mm and the thickness used for the two layers of paint was 4.5mm. They were different stainless steel samples therefore comparisons could not be made.

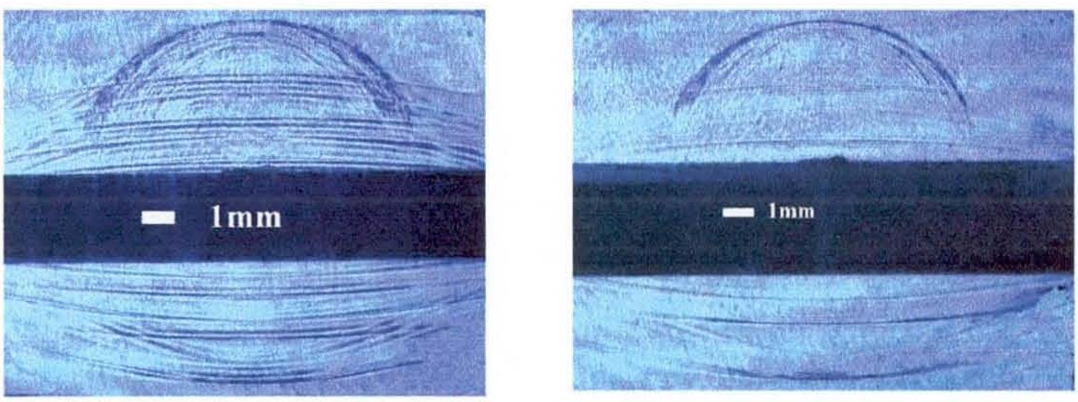

a b

Figure 6.5 Stainless steel painted once (**a**) and twice (**b**) for time delay 3.5μs. Stainless steel in **a** have a thickness of 3.14mm and the one in **b** have a thickness 4.5mm.

6-3-3 Conclusion

Section 6-3-1 and 6-3-2 shows the results obtained with single and double thickness of paint on both copper and stainless steel. Enlarged versions of the secondary shock waves are shown in figure 6.6 for copper and figure 6.7 for stainless steel. The separation of the secondary shock waves obtained for one and two layers of paint on the surface of copper was about 0.16mm and 0.10mm respectively. For stainless steel the separations were 0.21mm and 0.11mm respectively for one and two layers of paint. The table 6.1 gives a summary for the frequency of these secondary shock waves as a function of paint thickness.

The results clearly suggest that the thickness of the paint layer is important in the separation of the fringes and may be even in the generation. From simple physics, the separation obtained for the two metals could have been explained if a smaller separation was obtained for a thinner layer of paint than for a thicker, in this case the opposite happens. Both experiments for the one layer of paint on the surface of copper and stainless steel were carried out on the same day. The experiment with two layers of paint on the surface of copper and stainless steel was carried out on a different day. For both of the experiments, the variables in the process have been kept constant apart from the paint thickness and the thickness of the metal.

From these experiments, significant conclusions can not be made. It has been seen that the paint thickness has an effect on the separation of the secondary shock waves. Conclusions can not be drawn from the current results, on the effect of paint layer on the secondary shock wave separations. It does seem that increasing the paint thickness decreases the separation (increases the frequency).

Metal	Frequency approximation in MHz
Copper Painted Once	8
Copper Painted Twice	15
Stainless steel Painted Once	7
Stainless steel Painted Twice	14

Table 6.1 Separation of Secondary shock waves as a function of paint thickness.

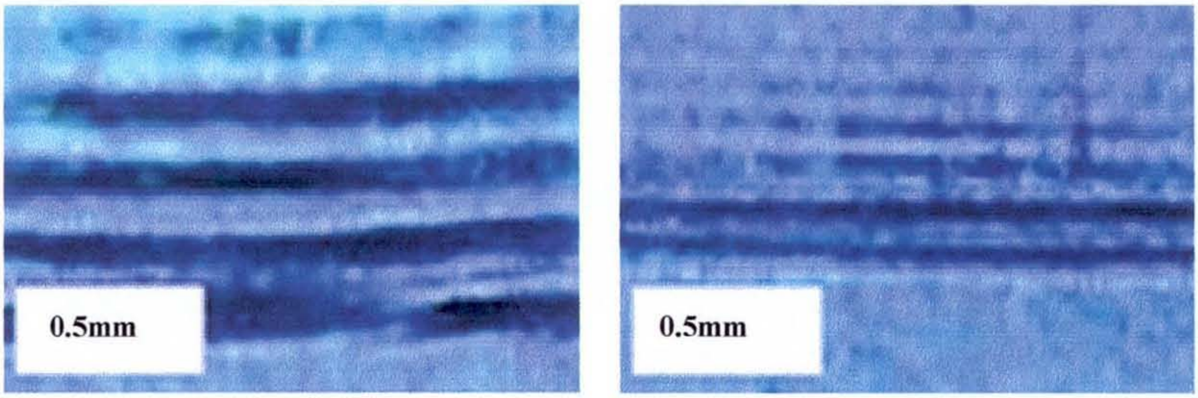

a b

Figure 6.6 a) Secondary shock waves from a piece of copper (thickness of 3.14mm) painted once. **b)** Secondary shock waves obtained with a piece of copper (thickness 4.47mm) painted twice.

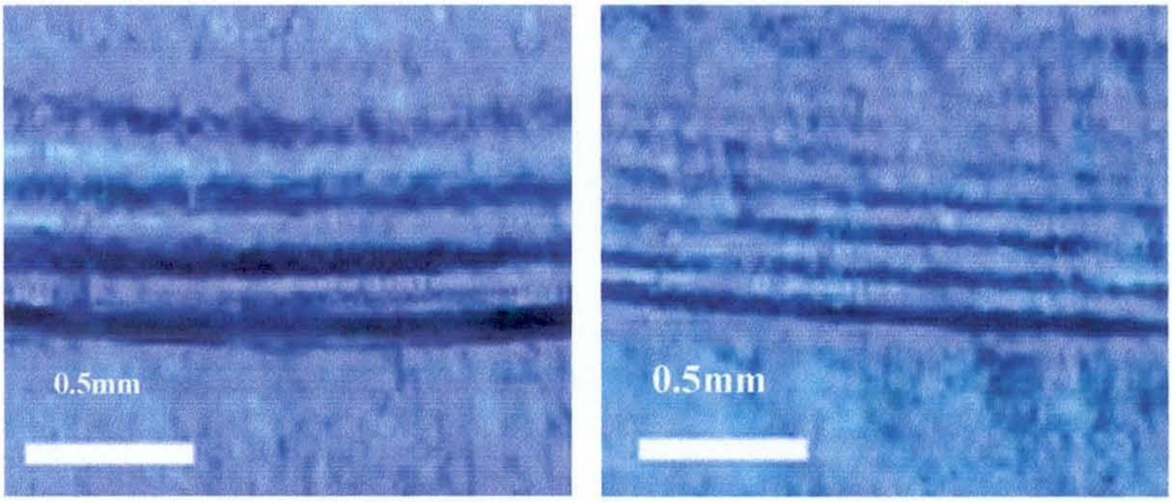

a b

Figure 6.7 a) Secondary shock waves from a piece of stainless steel (thickness 3.14mm) painted once, and **b)** secondary shock waves obtained from a piece of stainless steel (thickness 4.5mm) painted twice.

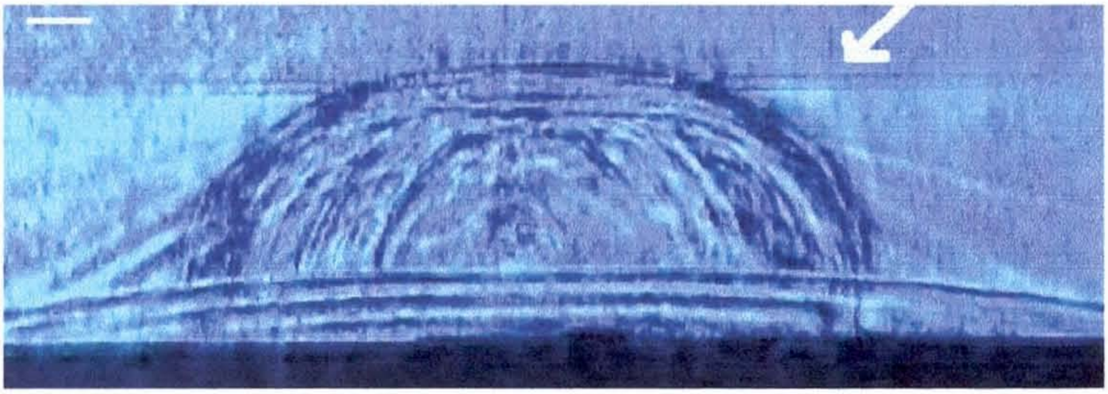

Figure 6.8 Stainless steel time delay 2.5μs, with one layer of paint. It shows two fringes produced due to the layer of paint.

Figure 6.8 shows the flat shock wave produced above the surface of the metal as explained in section 4-4-3. The arrow in the figure points out two fringes which are present behind the flat wave. This flat wave is caused by the scattered laser light being focused at the surface of the metal and hitting a larger area of the paint. The same laser paint interaction process as explained in section 4-4-1 takes place. The first flat shock wave is produced as the laser beam hits the layer of paint, the second flat wave, which follows the first is believed to be the reflection of the first wave from the surface of the metal. The separation of it is a function of the paint thickness.

6-4 Secondary Shock wave in different metals

Secondary shock waves were obtained with various different metals when the laser shock peening process was applied. Table 6.2 gives the frequency of the secondary shock waves for various metals, with the speed of sound (for P-waves) and the density of the respective metals. Figure 6.9 shows Schlieren pictures of brass, titanium, lead and aluminium where secondary shock waves are seen. The secondary waves generated on brass and titanium are similar to the ones seen on copper or stainless steel. The primary and secondary shock waves on lead are confined to one region, and the waves seem to lose intensity as a function of reflection. This may be due to the softness and the malleable nature of the metal.

From the table below it can be concluded that the separation of the secondary shock waves is also dependent on the metal used in the peening process. The frequency of the secondary shock waves with a particular metal doesn't seem to be related to velocity of sound or density of the metal. More work has to be carried out in order to come to firm conclusions. Suggestions for further work are mentioned in chapter 7.

Metal	Frequency approximation of secondary shock waves in MHz	Density ($g\ cm^{-3}$)	V ($mm\ \mu s^{-1}$)
Aluminium	8	2.7	6.42
Brass	12	8.6	4.7
Copper	8	8.93	4.76
Lead	10	11.4	2.16
Stainless steel	7	7.9	5.79
Titanium	17	4.5	6.07

Table 6.2 Frequency of secondary shock waves for different metals.

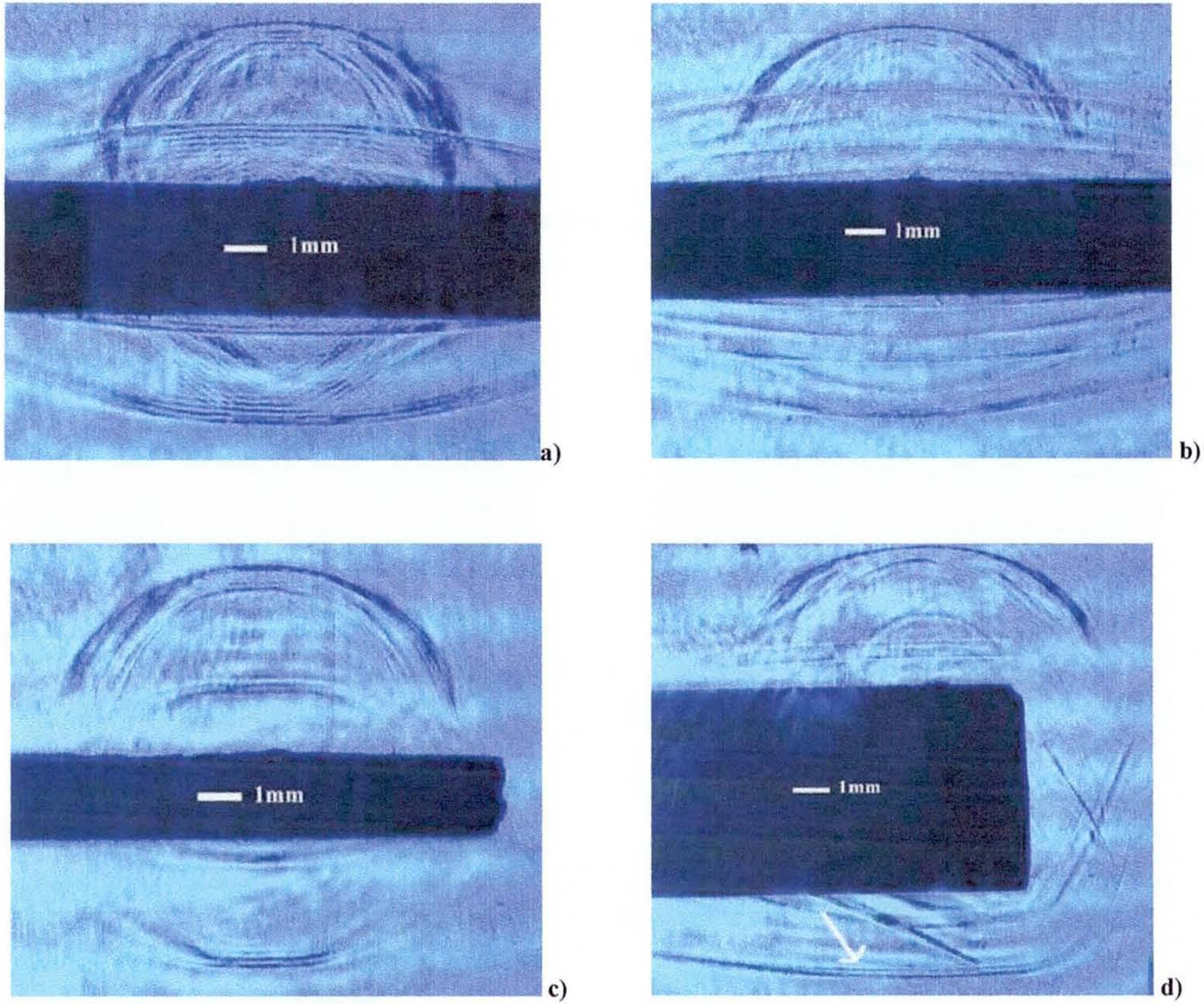

Figure 6.9. a) Brass, b) Titanium Un-peened, c) Lead and d) Aluminium. All the metals are painted once on the surface.

6-5 Effect of Previous Peening on the Secondary shock waves.

When a piece of titanium which has already been peened by Metal Improvement Company at Derby on one side and not on the other was subject to Laser shock peening, it was observed from the high speed Schlieren photographs that the peened and un-peened sides give different results with regards to secondary shock waves. The secondary shock waves were only seen on the un-peened side and the peened side only showed the primary shock waves. The piece of titanium was peened in an industrial environment and painted with the same paint on both sides.

The same experiment was carried out with a piece of copper which has been treated in a similar way. The peening on the piece of copper was done with a high power carbon dioxide laser (Model L450 Class 4 laser) as part of a final year project. The carbon dioxide laser was fired on eight 3mm square areas fifty times. It also showed similar results compared with titanium. The peened and the un-peened side have an effect on the generation of the secondary shock waves. Figure 6.10 shows the high speed Schlieren images obtained for titanium and copper for both peened and un-peened sides with a section of the picture where secondary shock waves are to be seen, enlarged. The fringe separation for both titanium and copper was the same as the ones shown in table 6.2.

This difference in peened and un-peened side with regard to the generation of the secondary shock waves has to be investigated further in order to make definite conclusions. The secondary shock waves may also be generated due to the softness of the metal before peening is applied. This experiment may suggest that the effects of the secondary shock waves are seen as a combined effect of the material properties and the paint layer.

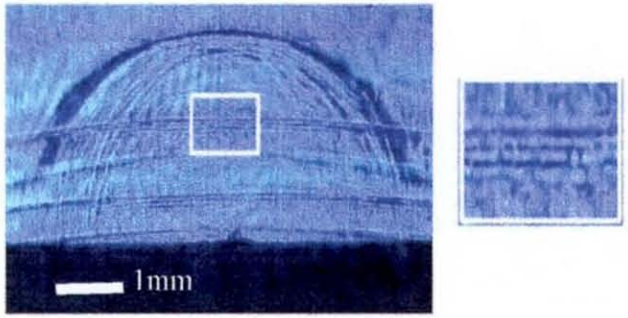

a) Titanium un-peened surface with a time delay of 2.5 μs Second and one layer of paint.

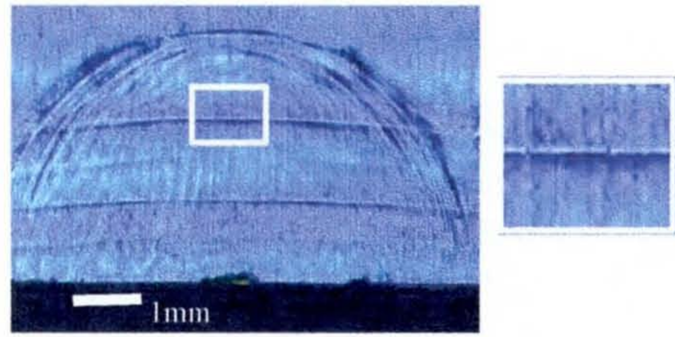

b) Titanium peened surface with a time delay of 2.5 μs and with one layer of paint.

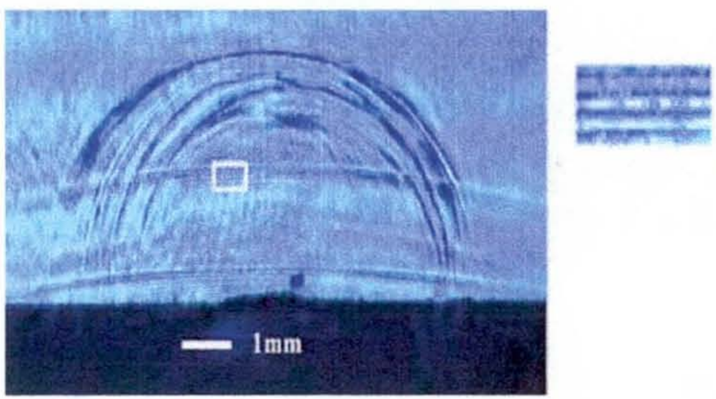

c

c) copper un-peened with one layer of paint and a time delay of 2 μs.

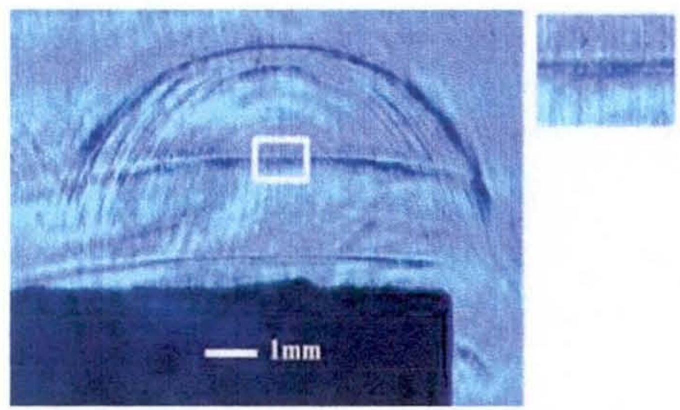

d) copper peened surface with one layer of paint at a time delay of 2 μs.

Figure 6. Generation of the secondary shock waves when LSP is applied on the peened and un-peened surfaces of copper and titanium.

6-6 Summary

This chapter has introduced the phenomenon of secondary shock waves seen when laser shock peening is applied to different metals. This was an unexpected discovery which led to some experimental work in order to investigate this effect. It was believed that the generation of these waves below the primary shock wave was due to the hardness of the metal and/or the layer of paint on the surface of the metal. Investigations were carried out with one and two layers of paint in order to try and see the effect it had on the secondary shock waves. The metal hardness and previous treatment was also investigated. With the few experiments carried out due to the limited amount of time, definite conclusions can not be made. Chapter 7 suggests further work in order to try to characterise these secondary shock waves.

CHAPTER 7

Conclusions and Further work

The work presented in this thesis examines the interaction of an intense laser pulse with the surface of a metal in the laser shock peening process. When laser shock peening is applied to a metal surface, an ablation shock wave is produced which, depending on the geometry and laser beam area, induces residual stress in the surface layer of the metal. This ablation shock wave is visualised using high-resolution Schlieren photographs of the process at different times. Cavitation was also investigated in Chapter 3 as part of the initial schlieren experiment. The formation and collapse of a laser generated cavitation bubble during the first oscillation cycle was showed by employing high-speed photography and a thin film PVD pressure transducer. This phenomena has been investigated in previous research work, and the purpose of carrying it out in this thesis was to test the high-speed photographic system and synchronisation of the equipment described in chapter 2 and to compare the validity of the results obtained with published ones. The results obtained agree with the ones already published. The radius of the generated bubble and the oscillation time period for one cycle was dependent on the energy density of the laser pulse used. As a consequence direct comparison to previous results could not be made but theory was proven to be correct.

Laser shock peening experiments carried out in this thesis were set up and performed in order to try and confirm previous theories and to get a better understanding of the shock formation in the laser-paint-metal-water interaction. The process was performed on different metal samples in order to obtain results as a function of material properties. When applied to stainless steel shims it was observed that the frequency of shock waves generated in water was a function of the metal thickness as given by simple theory. Different metals samples from 0.4mm - 1.27mm have been used and the results obtained coincide with the theoretical calculations.

The Schlieren photographs taken of the interaction process also showed an interesting phenomenon, which was not expected. This was the generation of the secondary shock waves below the primary shock as explained in chapter 6. Definite conclusions for why the formation of the secondary shock waves could not be made from the results obtained. It was also observed that the properties of the secondary waves changed as a function of paint thickness and metal. More experimental work is needed in order to understand this phenomenon and draw conclusion from it. The formation of the secondary shock waves was not possible to be investigated further in this thesis due to the one-year funding of the project.

Further work should be carried out in order to investigate the formation of the secondary shock waves and get an understanding of their formation. In this thesis it was observed from the Schlieren photographs taken that the paint layer on the metal surface and also the different properties of the metals have an effect on the secondary shocks. Further work should be carried out in order to understand what effect the paint layer has on the secondary shock waves. The paint used in these experiments was Halfords Ford Black professional car paint. Different paints may be investigated with different number of layers in order to see the effect it has on the secondary shock waves.

Further observations might be conducted on different metal samples to see if the results correlate with the ones obtained. The investigation of the secondary shock wave formation on different materials, such as plastics, which have different properties to metals might be interesting.

Publications
Articles and conference papers

Journals

- Don Liyanage D. K. L. and D. C. Emmony, "Schlieren images of laser-generated ultrasound" Applied Physics Letters, Volume 79, Number 20 (2001).

Conference

- The Association for High Speed Photography and Photonics Annual Conference at Harrow, United Kingdom, September 2001. An oral presentation was given under the title "Optical diagnostics of the laser hardening process".